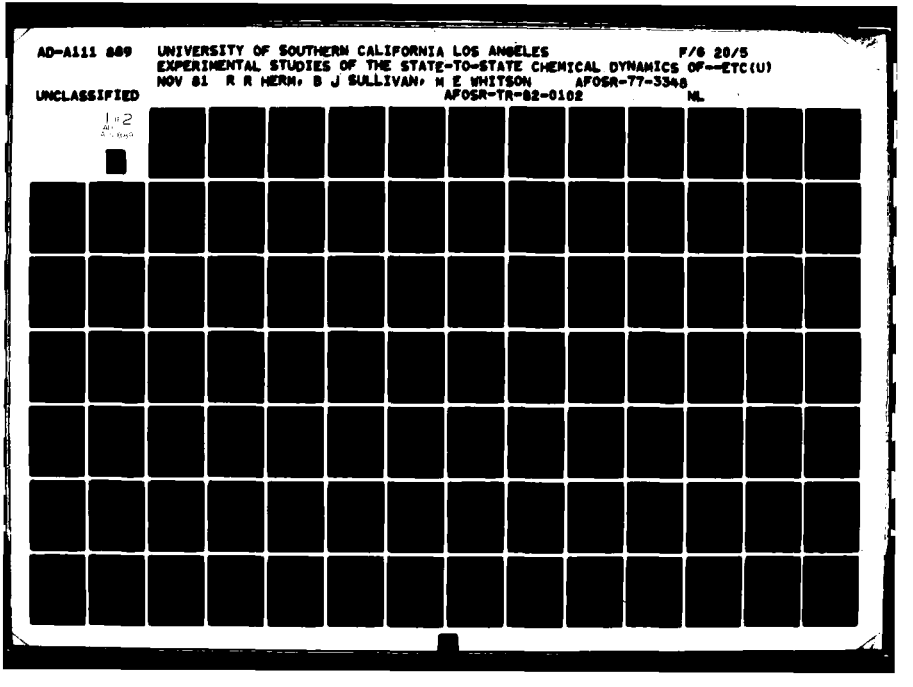
AD-A111 889
UNIVERSITY OF SOUTHERN CALIFORNIA LOS ANGELES F/G 20/5
EXPERIMENTAL STUDIES OF THE STATE-TO-STATE CHEMICAL DYNAMICS OF--ETC(U)
NOV 81 R R HERM, B J SULLIVAN, M E WHITSON AFOSR-77-3348
UNCLASSIFIED AFOSR-TR-82-0102 NL
1 of 2

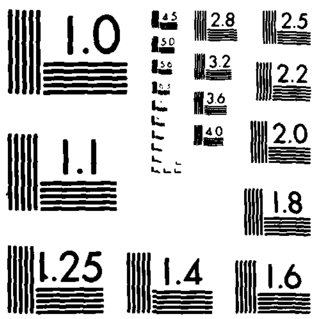

MICROCOPY RESOLUTION TEST CHART
NATIONAL BUREAU OF STANDARDS-1963-A

Unclassified
SECURITY CLASSIFICATION OF THIS PAGE (When Data Entered)

REPORT DOCUMENTATION PAGE

READ INSTRUCTIONS BEFORE COMPLETING FORM

1. REPORT NUMBER: AFOSR-TR- 82-0102	2. GOVT ACCESSION NO.: AD-A111889
3. RECIPIENT'S CATALOG NUMBER:	
4. TITLE (and Subtitle): Experimental Studies of the State-to-State Chemical Dynamics of Reactions Involving Air Triatomics	5. TYPE OF REPORT & PERIOD COVERED: Final Report
	6. PERFORMING ORG. REPORT NUMBER:
7. AUTHOR(s): R. R. Herm, B. J. Sullivan, M. E. Whitson, Jr.	8. CONTRACT OR GRANT NUMBER(s): AFOSR-77-3348
9. PERFORMING ORGANIZATION NAME AND ADDRESS: University of Southern California, University Park, Los Angeles, CA 90007	10. PROGRAM ELEMENT, PROJECT, TASK AREA & WORK UNIT NUMBERS: 61102F, 2303/B1
11. CONTROLLING OFFICE NAME AND ADDRESS: Air Force Office of Scientific Research/NC, Bolling AFB, DC 20332	12. REPORT DATE: 1 Nov. 1981
	13. NUMBER OF PAGES: 99
14. MONITORING AGENCY NAME & ADDRESS(if different from Controlling Office)	15. SECURITY CLASS. (of this report): Unclassified
	15a. DECLASSIFICATION/DOWNGRADING SCHEDULE

16. DISTRIBUTION STATEMENT (of this Report)

Approved for public release; distribution unlimited.

17. DISTRIBUTION STATEMENT (of the abstract entered in Block 20, if different from Report)

18. SUPPLEMENTARY NOTES

19. KEY WORDS (Continue on reverse side if necessary and identify by block number)

Nitric Oxide

Vibrational Excitation

Laser Induced Fluorescence

20. ABSTRACT (Continue on reverse side if necessary and identify by block number)

The first measurements of the full vibrational distribution of NO produced in the room temperature reaction

$$N(^4_U S) + O_2^n \rightarrow NO\ (0 \leq v \leq 7) + O \qquad (1)$$

are reported in this work. The technique of UV laser induced fluorescence detection of NO(v) was employed, which permitted observation of NO production under conditions where O_2 vibrational quenching of the NO(v)

(Continued on Back)

DD FORM 1 JAN 73 1473 EDITION OF 1 NOV 65 IS OBSOLETE S/N 0102-LF-014-6601

UNCLASSIFIED

SECURITY CLASSIFICATION OF THIS PAGE (When Data Entered)

20. ABSTRACT (Continued)

was insignificant. The technique permitted the first observation of NO(v=0) and NO(v=1) concentrations.

The relative ratios of $[NO(v)]/k_D^v$ were measured, where k_D^v is the vibrationally dependent rate of NO removal by the reaction

$$N(^4S) + NO(v) \xrightarrow{k_D^v} N_2 + O.$$

Assuming that k_D^v is independent of v, we calculate that the NO vibrational distribution ratios for $0 \leq v \leq 7$ are

57.8: 4.2: 5.7: 6.9: 5.8: 6.5: 6.6: 6.5,

expressed as % of total NO production. This result indicates that the $N(^4S) + O_2$ reaction produces 42% of the NO molecules in infrared-active states, 38% of them in levels ≥2. In terms of energy deposition, 29% of the 1.39 eV exothermicity of the reaction goes into $v \geq 1$, 28% into $v \geq 2$; this is ~3 times more than predicted by earlier studies.

The observed NO(v) ratios are in fact the nascent production ratios if vibrational relaxation of NO(v) by N atoms occurs with a rate much smaller than the rate of removal of NO(v) by reaction with N atoms. Assuming that N atom quenching is insignificant we calculate the set of rate coefficients k_1^v, for $0 \leq v \leq 7$, to be 52., 3.8, 5.1, 6.2, 5.2, 5.9, 5.9, 5.9 in units of 10^{-18} cm^3 molecule^{-1} sec^{-1}. If rapid N atom quenching occurs, production of infrared active states of NO by the $N(^4S) + O_2$ reaction is even more efficient than these rates indicate.

(12)

Final Report

Experimental Studies of the State-to-State Chemical Dynamics of Reactions Involving Air Triatomics

Prepared by

R. R. Herm, B. J. Sullivan, and M. E. Whitson, Jr.
Chemistry and Physics Laboratory

1 November 1981

The Ivan A. Getting Laboratories
The Aerospace Corporation
El Segundo, California, 90245

Prepared for

Directorate of Chemical Sciences
AFOSR, Bolling AFB
Washington, D. C.

[redacted] AFOSR-77-3348

Final Report
Experimental Studies of the State-to-State
Chemical Dynamics of Reactions Involving
Air Triatomics

Prepared by:

R. R. Herm B. J. Sullivan M. E. Whitson, Jr.

Approved:

S. Feuerstein Director
Chemistry and Physics Laboratory

Table of Contents

		Page
	Abstract	1
I.	Introduction	3
II.	Experimental	5
	1. Kinetic Constraints	5
	2. Spectroscopic Considerations	7
	3. Apparatus and Reagents	11
	4. Data Acquisition Techniques	18
III.	Results	23
	1. ϕ Variation as a Function of O_2 Partial Pressure	23
	2. NO(v) Ratios	25
	3. Fluorescence Efficiencies	25
	4. Thermal Equilibrium Studies	27
	5. Absolute Value of NO(v=1) Concentration	29
IV.	Discussion	31
	1. Appropriate Kinetic Models	31
	2. Comparisons with Other Studies	38
	3. Implications of This Work for Atmospheric Radiance Models	40
V.	Conclusions and Recommendations	42
VI.	References	44

List of Tables

Table Title

1. Franck-Condon Factors and Approximate Wavelengths for Selected NO γ-Bands
2. Dyes and Crystals used in the LIF System
3. Observed NO(v) LIF Signals as a Function of O_2 Partial Pressure, Uncorrected for Fluorescence Efficiency
4. Observed NO(v) Distributions: Low Pressure and at 400 mTorr of O_2
5. Comparison of Observed and Calculated NO(v) Bandhead Ratios
6. Relevant Chemistry used in the Kinetic Modeling
7. Calculated Flowtube Composition for 50 mTorr and 400 mTorr O_2 Partial Pressure
8. O_2 Quenching Rate Coefficients, and the Calculated NO(v) Ratios Based on those Coefficients at 400 mTorr O_2 Partial Pressure
9. Comparison of NO($v > 2$) Distributions Measured in Different Studies
10. Comparison of Selected Kinetic Parameters for this Work and Previous IR Chemiluminescence Studies
11. Einstein Transition Probabilities for $NO(X^2\Pi, v)$ $\Delta v=1$ and $\Delta v=2$ IR Transitions
12. Atmospheric Parameters of an IBC Type I Aurora

List of Figures

Figure

1. Energy Level Diagram for the $N(^4S) + O_2$ Reaction
2. Electronic Energy Diagram of the NO Molecule
3 to 10. Calculated Spectral Excitation Profiles: NO $\gamma(0,0)$ through $\gamma(0,7)$
11. Schematic Diagram of the Apparatus
12. Spectral Response Characteristics of the ITT Vacuum Photodiode
13. Spectral Response of the EMR 542 Q Solar-Blind Photomultiplier
14. Pulse Pileup Correction Factors
15. Comparison of the Observed $\gamma(0,3)\ ^2\Pi_{1/2}$ Bandheads and the Spectrum Calculated Assuming 300° Rotational Equilibrium
16 to 23 Experimental Results: Observed Variation in the NO(v) LIF Signal as a Function of O_2 Partial Pressure, for v=0 through v=7
24. Observed NO Vibrational Distributions
25. Observed change in LIF Signal from a Constant Concentration of NO, as the O_2 Partial Pressure is Varied
26. Fluorescence Efficiency Correction Factors
27. Surprisal Plot of the $N(^4S) + O_2$ Reaction
28. Rate Coefficients for the NO(v) + O_2 Quenching Process
29. Comparison of $\phi(v=0)$ Data Corrected using Two Values of k_{15}.
30. Comparison of Vibrational Distributions from This and Other Studies

Abstract

The first measurements of the full vibrational distribution of NO produced in the room temperature reaction

$$N(^4S) + O_2 \rightarrow NO\ (0 \leq v \leq 7) + O$$

are reported in this work. The technique of UV laser induced fluorescence detection of NO(v) was employed, which permitted observation of NO production under conditions where O_2 vibrational quenching of the NO(v) was insignificant. The technique permitted the first observation of NO(v=0) and NO(v=1) concentrations.

The relative ratios of $[NO(v)]/k_D^v$ were measured, where k_D^v is the vibrationally dependent rate of NO removal by the reaction

$$N(^4S) + NO(v) \xrightarrow{k_D^v} N_2 + O.$$

Assuming that k_D^v is independent of v, we calculate that the NO vibrational distribution ratios for $0 \leq v \leq 7$ are

57.8: 4.2: 5.7: 6.9: 5.8: 6.5: 6.6: 6.5,

expressed as % of total NO production. This result indicates that the $N(^4S)$ + O_2 reaction produces 42% of the NO molecules in infrared-active states, 38% of them in levels >2. In terms of energy deposition, 29% of the 1.39 eV exothermicity of the reaction goes into $v \geq 1$, 28% into $v \geq 2$; this is ~ 3 times more than predicted by earlier studies.

The observed NO(v) ratios are in fact the nascent production ratios if vibrational relaxation of NO(v) by N atoms occurs with a rate much smaller than the rate of removal of NO(v) by reaction with N atoms. Assuming that N atom quenching is insignificant we calculate the set of rate coefficients k_1^v, for $0 \leq v \leq 7$, to be 52., 3.8, 5.1, 6.2, 5.2, 5.9, 5.9, 5.9 in units of 10^{-18} cm^3 $molecule^{-1}$ sec^{-1}. If rapid N atom quenching occurs, production of infrared active states of NO by the $N(^4S) + O_2$ reaction is even more efficient than these rates indicate.

I. Introduction

Reaction rate data for processes which occur in the upper atmosphere have become increasingly important to the Air Force over the last two decades. These processes, many of which involve atoms and simple atmospheric diatomic and triatomic species, alter atmospheric density and composition, and often result in emission of visible and infrared radiation. A detailed understanding of these processes is required for modeling natural atmospheric radiance and post-nuclear-burst emissions. Experiments which are state specific in both reactants and products are now required to obtain chemical kinetic data for radiance codes, and such experiments are at the present frontier of chemical kinetic research.

The development in recent years of the hardware required to do state-specific chemical research, such as tunable lasers, non-linear optics, and sophisticated photon detectors, has made a new set of molecular and atomic species tractable for quantitative laboratory studies. The Air Triatomics project was initiated in June, 1977, in recognition of the fact that this new technology permitted state-specific study of NO produced in key atmospheric reactions.

We present here the first measurements of the full vibrational distribution of the NO produced in the reaction

$$N(^4S) + O_2(X\ ^3\Sigma^-_g) \xrightarrow{k_1} NO(X^2\Pi, v) + O(^3P), \qquad (1)$$

which has an exothermicity, ΔE, of 32 kcal/mole and an activation barrier, E^*, of 7 kcal/mole [1]. Vibrational levels up to and including v=7 are permitted by the total available energy $E^* + \Delta E$. The energy level diagram for the $N(^4S) + O_2$ reaction is given in Fig. 1. Sufficient energy is not available for other reaction paths, such as production of $O(^1D)$, to occur.

Three theoretical studies of the $N(^4S) + O_2$ reaction potential energy surfaces exist in the literature: ab initio calculations by Benioff et al. [2,3] and a semi-empirical calculation by Wilson [4]. None address the problem of energy deposition within the NO vibrational manifold.

The overall reaction rate coefficient, k_1, has been measured by Kistiakowsky and Volipi [5], Clyne and Thrush [6], Clark and Wayne [7], and others [1]. Efforts to obtain vibrational state specific reaction rate coefficients for reaction (1) include low resolution work by Hushfar et al. [8] which clearly indicated NO(v) production up to $v \leq 7$, Whitson et al. [9], which reported the relative production of NO(v) for NO($2 \leq v \leq 7$) and the higher resolution work of Rahbee and Gibson [10], which produced more accurate values of the relative production of NO ($2 \leq v \leq 7$) and an estimate of the state specific reaction rate coefficients. All of these techniques used first overtone infrared measurements of NO(v) and thus were limited to observations of only NO($v \geq 2$). In addition, the sensitivity of the infrared technique restricted observations to conditions in which the O_2 partial pressure was high enough to cause significant vibrational quenching of NO(v) [8,9,10], requiring extensive kinetic modeling efforts to calculate nascent NO(v) distributions from experimental data.

This report is the final summary of the Air Triatomics project. The first use of UV laser induced fluorescence detection (LIF) for studies of NO vibrational-state-specific kinetics is described here. The experimental apparatus, results, and analysis techniques are detailed in subsequent sections.

II. Experimental

1. Kinetic Considerations

Previous studies of the $N(^4S) + O_2$ reaction [8,9,10] were performed at relatively high pressures of O_2, since this was required for producing sufficient populations of NO(v) to detect using infrared chemiluminescent techniques. The role of the quenching process

$$NO(v_i) + O_2 \xrightarrow{k_2^v} NO(v_f < v_i) + O_2 \qquad (2)$$

in determining the observed NO distribution under typical IR experimental conditions was first recognized by Whitson et. al. [9], who estimated a set of O_2 quenching rate coefficients and applied these to deducing the nascent NO vibrational production of reaction (1) from a highly quenched NO vibrational distribution. The first measurement of the quenching coefficient k_2^1 was made by Murphy et al. [11], who obtained a value of $(2.4 \pm 1.5) \times 10^{-14}$ cm^3 molecule^{-1} sec^{-1}, and later by Fernando and Smith [12], who reported $(2.9 \pm .5) \times 10^{-14}$ cm^3 molecule^{-1} sec^{-1}, and by others [13,14], with similar results. Recently preliminary values of k_2^v have been obtained by Caledonia et al. [15], which indicate that quenching effects are even more pronounced that had been thought. For $v > 2$, in fact, $k_2^v > 10^{-13}$ cm^3 molecule^{-1} sec^{-1}, resulting in a characteristic quenching time of <.3 msec at 1 Torr of O_2. Thus O_2 quenching is the predominant mechanism for determining the observed NO vibrational distribution in all infrared chemiluminescent experiments performed to date. The extreme sensitivity of the LIF system described here allows study of NO(v) production at very low O_2 concentrations. For $[O_2] < 50$ m Torr the NO(v) produced by

$$N(^4S) + O_2 \rightarrow NO(v) + O \qquad (1)$$

and lost by process (2) and the reaction

$$N(^4S) + NO(v) \xrightarrow{k_3} N_2 + O \qquad (3)$$

reaches a steady state in which the effect of process (2) is negligible, and

$$[NO(v)]_{ss} = \frac{k_1^v}{k_3} [O_2]. \qquad (4)$$

Thus, measurements of $[NO(v)]_{ss}$ in the $O_2 \leq 200$ m Torr range should directly yield the nascent vibrational concentrations of NO, assuming k_3 is not a function of v and that the NO(v) is not quenched rapidly by N atoms.

All studies of reaction (1) which attempted to determine vibrational branching information, have assumed that k_3 is independent of the NO vibrational level involved. For $v = 0$, reaction (3) proceeds at ~.1 times the gas kinetic rate [16], and it is reasonable to assume that vibrational energy would have a minimal effect on the process, since the activation energy for reaction (3) is very small or zero [16]. Our measurements are rigorously of the ratios of k_1^v/k_3^v for $0 \leq v \leq 7$, and our reported low pressure distribution is based on the assumption that $k_3^v = k_3$. In the event that k_3^v is ever measured, the distribution reported here should be reevaluated.

The actual kinetic system in either a flowtube system as used here or an integrating sphere as used in the infrared work, is far more complex than just equations 1,2, and 3. Copious quantities of O atoms are produced at high O_2 concentrations, especially in integrating spheres, where the residence time of the reagents is long compared to the NO lifetime in the system. O atoms are

known to quench NO(v) rapidly [17,18], thus complicating the analysis of data obtained with more than a few hundred mTorr of O_2 present in the reaction zone.

2. Spectroscopic Considerations

All NO(v) measurements reported here were made using the NO γ-Band system from 226nm to 316nm (γ(0,0) to γ(0,7)). The γ-Bands are spectroscopically complex, arising from $X\ ^2\Pi - A^2\Sigma$ transitions shown in Fig. 2, with 123 cm^{-1} spin orbit splitting of the $X^2\Pi$ state [19]. The resulting structure of each band is similar to γ(0,0), shown in Figure 3, with a total of 12 overlapping branches, 4 pairs of which are unresolved owing to the small spin splitting of the upper state.

The γ system is unusually appropriate for doing LIF kinetic studies, as it has a wide spacing between bands and a radiative lifetime sufficiently short to avoid severe electronic quenching by flowtube constituents. Table 1 presents the Franck-Condon factors for the γ-Bands along with the approximate $^2\Pi_{1/2}$ bandhead wavelengths.

The spectral emission profile of the laser used for the LIF studies is sufficiently narrow that the γ-band structures observed, which are generally groups of lines, are generally separated, providing ranges within the LIF spectrum where the system background can be observed. Furthermore, the bandhead structures are sufficiently well defined that identification of the LIF spectrum is straightforward.

The $A\ ^2\Sigma$ state which is the state to which the NO(X,v) is excited in the LIF process, has a lifetime of 200 nsec [20] from its v=0 level. Transition probabilities for γ(0,0) through γ(0,7) were sufficiently large that all LIF studies were made to this $A^2\Sigma$, v=0 level. This is significant because the A state of NO is quenched very rapidly by O_2, and the partial pressure of O_2 is adjusted in this work from ~10 mTorr to 400 mTorr. This quenching rate coeffi-

cient is approximately 1.8×10^{-10} cm^3 $molecule^{-1}$ sec^{-1}, as determined in this lab and described in a subsequent section, so O_2 partial pressures in excess of ~ 100 mTorr result in a considerable reduction in the fluorescence efficiency of the LIF process. However, only ratios of LIF signals from the different NO vibrational levels are required in order to derive the full set of relative NO vibrational population ratios at a given O_2 partial pressure, since all NO(X,v) levels are excited to the same NO(A,v=0) level and hence are observed with the same fluorescence efficiency.

Final analysis of the NO LIF data to obtain NO vibrational population ratios requires detailed spectroscopic knowledge of each band used, the spectral emission profile of the doubled dye laser, and the spectral response of the laser power measuring system. So long as no optical changes are made in the LIF system while two states are being ratioed, the phototube spectral response is not required; this is obvious when one considers that the fluorescence spectral content is a function of the upper ($A^2\Pi$) state, not of the $X^2\Sigma$ vibrational state excited. A computer code containing well-established NO γ-Band Franck-Condon factors and other spectroscopic constants (21,22) general coupling case Honl-London factors, and experimentally measured laser spectral bandpass was used to calculate the LIF spectra to be expected for 300°K rotational and spin-state equilibrium.

The general equation for the intensity of a line observed using laser induced fluorescence, see for example Tatum [23] or Shultz et al. [24], reduces to the simple form, normalized to unit laser input power,

$$I(v'J',\ r''v''J'') \propto N_{r''v''J''} * q_{v'v''} * \left(\frac{S_{J'J''}}{2J'' + 1}\right), \qquad (5)$$

where $N_{r"v"J"}$ is the population of $NO(X^2\Pi_r, v", J")$, which we assume to be in thermal equilibrium for the rotational and spin-orbit states, $q_{v'v"}$ are the Franck-Condon factors for the band, and $S_{J'J"}$ is the line strength factor. Note that no emission term for the NO(A) fluorescing state is required, since all lines excited in this work create the $NO(A^2\Sigma, v'=0)$ state.

Comparison of LIF data from different vibrational levels requires information concerning the shape of the excitation spectrum as a function of wavenumber. A synthetic LIF spectrum was produced for each vibrational level studied by calculating the individual line intensities, I(v'J',r"v"J") from equation (5) for each γ- Band and convoluting these lines with an experimentally determined laser spectral profile, $P(\nu)$. Identifying the i^{th} line of a gamma band as having intensity $I_i(\nu)$, where i identifies a specific combination of v',J',r",J", v", the required spectrum is defined by

$$\mathcal{I}(\nu) = \sum_{i=1}^{N} I_i(\nu')P(\nu-\nu') \qquad (6)$$

where N is the maximum number of lines considered for the calculation. For the synthetic spectra shown in Figures 3 to 10, N was 600, corresponding to the first 50 lines in each branch. $P(\nu-\nu')$ was determined by scanning the laser over a single line and analyzing the resulting LIF spectrum to get the apparent linewidth. A Gaussian profile was assumed, and a FWHM of 1.2 cm^{-1} was found to best match the spectrum; thus only a few lines contribute significantly to $\mathcal{I}$ at a given wavelength. Figures 3-10 use this laser profile, and assume unit laser input power and 300°K spin-orbit and rotational state equilibrium. The intensities thus obtained are correct relatively, and can be used for comparing two LIF spectra from different vibrational levels to get population ratios. The spectra were calculated using Franck-Condon factors from Flinn [21], Honl-London factors from Schadee [25,26], and the remaining constants from Englemann [22].

The data acquisition technique used to measure LIF intensities to be used for calculating NO(v) will be described in full in a subsequent section. Typically one or more of the bandheads, large or small, of the γ- Band under study was scanned, and these are composites of many individual spectral lines. Figures 3 through 10 are calculated to represent the LIF spectrum resulting from these lines, and listing all of the lines contributing to each bandhead is of little value. Table 2 is presented as an example of the underlying complexity of the band; this table shows the structure of the small $^2\Pi_{3/2}$ $\gamma(0,0)$ bandhead, the long-wavelength structure in Fig. 3. This bandhead is the simplest structure of the 12 branches in a γ band.

A final spectroscopic concern was the question of whether enough NO was made in the flowtube to cause a meaningful decrease in the optical depth in the flowtube. Significant absorption of $\gamma(0,0)$ conceivably occur: (1) in the 1.5 cm from the excitation zone in the fluorescence cell up to the phototube window; or (2), in the exit arm of the cell, 36 cm in length. Based on the data of Mohlman et al. [20], one obtains a concentration of $> 10^{14}$ molecules/cm^3 for case (1) to result in a 1/e decrease at the center of a line in $\gamma(0,0)$. If the entire exit arm of the cell had a concentration of NO(v=0) of $\sim 9 \times 10^{12}$ molecules/cm^3, a similar decrease would result. Both cases require much more NO(v=0) than exists in the flowtube. If all of the NO produced by reaction (1) were made in v=0, the maximum steady-state concentration in the flowtube under our 400m Torr O_2 conditions would be 3.5×10^{10} molecules/cm^3, by Eq. 4.

An experimental demonstration of the lack of $\gamma(0,0)$ absorption in the flowtube was performed, using a 1 cm long cell between the fluorescence cell and the photomultiplier. This cell was arranged so it could be filled with NO. The LIF signal from NO(v=0) produced under 400 mTorr O_2 conditions was observed to decrease by 24% when 1 Torr of NO was added to the absorption cell. When the

photomultipler response and the Franck-Condon factors for the γ-Bands are used to calculate the expected decrease, assuming all $\gamma(0,0)$ LIF signals are blocked by the NO in the absorption cell, the expected decrease is within 10% of that observed, demonstrating that the experiment is most certainly performed under optically thin conditions.

3. Apparatus and Reagents

The system used for the measurements reported here consisted of a frequency-doubled dye laser coupled to a conventional flowing afterglow apparatus, shown in Fig. 11. Nitrogen atoms were produced by partially dissociating pure N_2 in a 17 Watt 2450 MHz microwave discharge. The discharge was located 70 cm upstream from the point of O_2 addition in order to minimize back-diffusion of O_2 into the hot afterglow region and resultant production of unwanted species. The discharge was optically isolated from the reaction zone by 3 Wood's horns.

The atomic and molecular species present in a flowing afterglow such as this are well characterized. Initial concentrations of $N(^2P)$, and $N_2(A^3\Sigma_u^+)$ present in the hot pink afterglow region, vanish rapidly through the processes

$$N_2(A) + N \xrightarrow{k_7} N_2(X) + N, \qquad (7)$$

with K_7 = 5.E-11 cm^3 $molecule^{-1}$ sec^{-1} [27], and

$$N(^2P) + N_2 \xrightarrow{k_8} N(^4S) + N_2, \qquad (8)$$

with k_8= 1.5E-14 cm^3 $molecule^{-1}$ sec^{-1} [23]. At the start of the reaction zone, the reactions

$$N(^2D) + O_2 \xrightarrow{k_9} NO\ (X,v) + O, \qquad (9)$$

and

$$N(^2P) + O_2 \xrightarrow{k_{10}} NO(X,v) + O, \qquad (10)$$

with k_9 = 5.2E-12 cm^3 $molecule^{-1}$ sec^{-1} and k_{10} = 2.6E-12 cm^3 $molecule^{-1}$ sec^{-1} [28], effectively convert residual concentrations of N metastables to NO, which is itself quickly destroyed by reaction (3). $N_2(A)$ is thereafter created by N atom recombination and removed by N atom quenching, with a steady state concentration of ~1.E8 molecules/cm^3 resulting under conditions such as those used in this system [29]. Vibrationally excited N_2 is present throughout the system, with a vibrational temperature on the order of 2500 °K, corresponding to a reduction of ~4 for each N_2 vibrational level. Kinetic considerations, based on the known quenching rates for $N_2(v=1)$ by NO and [30,31] and O_2 [32], 2.2E-15 cm^3 $molecule^{-1}$ sec^{-1} and 6.E-17 cm^3 $molecule^{-1}$ sec^{-1}, respectively, indicate that no perturbation of the NO vibrational distribution can be caused by energy transfer from $N_2(v)$, or from $O_2(v)$ populated by v-v transfer from $N_2(v)$. The afterglow, therefore, constitutes a relatively pure means of studing the reaction of $N(^4S)$ with ground state O_2.

The nitrogen atom concentration produced in this work was ~ 2 x 10^{13} atoms/cm^3, measured directly by conventional NO chemiluminescence titration techniques [33]. This concentration was observed to be constant throughout the length of the flowtube with up to 2 Torr of O_2 partial pressure, as calculations based on Eq. (1) and (2) and the reasonable assumption of very low N atom wall losses would predict. The titrations were made using a PACE capacitance manometer calibrated using Wallace and Tiernan model FA160 pressure gauges which in turn were referenced to a mercury manometer. The volumes used for expansion

were measured to ~ 1% and appropriately chosen for maximum accuracy in the measurement. The accuracy of the N atom measurement is basically limited by the detection of green NO_2^* chemiluminescence signaling an overtitrated condition; this condition was detected by a photomultiplier tube and was reproducible to ~15%. Based on these system characteristics, an absolute accuracy limit of ~±50% is assumed to characterize the N atom concentration measurement.

High concentrations of N atoms are not beneficial in a system of this type, since, by Eq. (4) the NO concentration is independent of [N], in the steady state, and large concentrations of N thus result in large concentrations of O atoms. The O atoms have a largely unknown effect on the excited species in the flowtube, and combine with N to form electronically excited states of NO which contribute to the UV afterglow radiation. The concentration used for this work, 2×10^{13} atoms/cm^3, was the lowest level available at which the microwave power supply used for dissociating the N_2 would operate properly. This level produced only a very low level of afterglow background, and it removed NO(v) by reaction 3 so that the characteristic residence time of the NO(v) was ~ 1msec in the flowtube. This was significant for two reasons: (1) NO(v) was not deactivated significantly at the walls, since < 3% of the NO(v) lived long enough to diffuse from the flowtube volume, based on a diffusion coefficient of 45 cm^2/sec, a total pressure of 3.4 Torr, a wall deactivation rate corresponding to every collision, and the other system parameters mentioned in this report; (2) the short N atom lifetime minimized the effect of quenching of NO(v) by O, O_2, or other flowtube constituents, since they had to have an effect in 1 msec. Thus, the single concentration of N atoms was accepted as a good compromise of system requirements and was kept constant throughout the experiment.

The N_2, Ar, and O_2 used for this work were Air Products Corporation, Research Grade or equivalent, with > 99.996 % purity. Matheson Corporation Research Grade NO (> 98% pure) was used after purification by repeated distillation in glass. Prior to admittance into the flow system, the O_2, N_2, and Ar were passed through liquid N_2 traps, and the N_2 was further purified by passage through a 1m long 850°K copper-packed quartz furnace. A total mean pressure of 3.4 Torr was maintained in the 25 mm i.d. pyrex flowtube, of which ~.6 Torr was N_2 and the balance was Ar and O_2. Pressures were measured using the same calibrated Wallace and Tiernan gauges.

A linear flow velocity of ~28m/sec was maintained, resulting in a total reaction time of 30 msec for all measurements. Flow rates for the individual component gases were measured using Matheson rotameters (types 602 and 603) installed in the high pressure side of the gas proportioning system. Each rotameter was individually calibrated in place using a water displacement technique and also a separate gas expansion technique which used the entire flow system in its operating configuration. Calibration curves obtained by the two methods agreed well with each other and with the nominal gas-specific calibration curves supplied by Matheson. Partial pressures of Ar, O_2, and N_2 in the flowtube were calculated from the rotameter readings, and the total linear flow velocity was fixed by setting the appropriate rotameter conditions and throttling the flowtube pumpout system until the flowtube mean pressure was 3.4 Torr. These conditions were used for all of the studies of reaction (1) for several reasons. First, the reaction time, that is, the time from the point of O_2 addition into the flowtube up to the center of the fluorescence cell, was sufficiently long that transient problems from mixing or establishment of the pseudo-steady-state equilibrium were obviated. Second, the pressure was sufficiently high that wall effects due to diffusion to the walls were

insignificant, as the N atom destruction of the NO(v) was the predominant loss mechanism in the flowtube. Third, the pressures and flows were all easily measurable and controllable. And, finally, the amount of time and effort for measuring the NO vibrational ratios was so great that a set of standard operating conditions were a necessity.

The NO(v) was probed by a Molectron UV-1000/DL-100 laser system. The output from the dye laser was frequency doubled; the dyes and crystals used are listed in Table 3. The UV beam and the fundamental visible beam, which were nearly coincident, passed through the fluorescence cell shown schematically in Fig. 9. This fluorescence cell was equipped with 30 cm long black anodized arms, equipped with angled input and output windows and internal baffles with 4 mm diameter knife - edged holes spaced approximately every 25 cm down the arms. This arrangement suppressed the scattered laser light to a level at which it was not detectable with the cell evacuated, and not a severe background with 3.4 Torr of gas in the cell.

Calculation of the effects of walls and the baffled arms based on the conservative limit of plug flow in the flowtube and a diffusion coefficient of 45 cm^2/sec were performed using the diffusion code developed by Judeikis [34]. It was found that in our system neither the walls nor the arms of the fluorescence cell could substantially alter the NO vibrational distribution, since the NO(v) is destroyed by N atoms in ~1msec.

System UV energy output levels were ~1μ joule per pulse, with a pulse rate of 10 pulses/sec. A vacuum photodiode was positioned to observe scattered UV light from the N_2 pump laser, in order to generate a signal synced to the laser light pulse for triggering the photon counting system. The laser pulse duration was < 10 nsec and the system sync jitter obtained with the photodiode was observed to be < 5 nsec.

Relative UV output power was measured at the output end of the fluorescence cell using an optical system consisting of a quartz prism for dispersing the light and separating the UV component from the nearly collinear visible component of the laser, diverging quartz lenses, and an ITT vacuum photodiode (ITT Electro-Optical Products Division, Fort Wayne, Indiana) calibrated by ITT using a system traceable to the NBS. The calibration of this photodiode is given as the spectral response of the photodiode, $D(\nu)$, in Fig. 12. This quantity is essential for ratioing LIF signals resulting from different excitation wavelengths.

Photodiode output pulses were amplified and stretched, sampled by a PAR Model 162 boxcar averager, and digitized. The mean number of digital counts per specified number of laser shots (usually 500 to 10,000), was preserved on punched paper tape along with the number of fluorescence photons observed for the same period. The linearity of this intensity measuring and recording system was checked frequently during data acquisition runs using calibrated filters for beam intensity attenuation.

Fluorescence was measured using an EMR 542Q solar-blind photomultiplier; Fig. 13 shows the spectral sensitivity for this specific device supplied by EMR. The tube was mounted on the fluorescence cell at right angles to the flowtube and the laser optic axis, and observed through a quartz lens a fluorescence zone approximately 10 mm in length. The photomultiplier pulses were transmitted to conventional fast NIM-type photon counting modules through 50 cm of RG-58C/U coaxial cable, shielded by copper tubing for noise suppression. The high voltage input to the tube was similarly shielded. The individual NIM modules had $\leq$ 10 nsec time resolution, and the operational system had a ~18 nsec pulse-pair resolution. For this reason, care was exercised to limit the fluorescence photon flux to $<$ 1 photon/shot in order to avoid the necessity of making large photon pile-up corrections to the data.

The photon counting system was used in a delayed-window mode. After a delay of 83 nsec, measured from the laser pulse, the counting system was gated on, which eliminated most RF noise pulses generated by the laser and also the peak fluorescence signal where the photons were too closely coincident to be resolved by our system. The photons were counted for the next 490 nsec, which is approximately twice the radiative lifetime of the NO(A) state. The system then was gated off, to minimize counts from the ever-present NO γ and δ band radiation arising from the N + O + M recombination process.

Photon counting systems have inherent count rate limitations based upon the photon pileup and system deadtime, the time after responding to a pulse during which the system cannot register another pulse. Given a true average count rate, R, which results from the activity while the system is gated on, not the much longer time when counts are disallowed, and a system deadtime, τ, the average rate of resolvable pulses, R', is given by [35]

$$R' = Re^{-R\tau}. \tag{10}$$

Equation (10) can be applied to a decaying fluorescence signal sampled by a gated counting system. The numerical approach is to separate the mean actual count rate for the window into N equal segments, each having a mean emission rate which is very nearly equal to the actual decaying emission rate for that period of time. For the N segments then, the CW equation above can be applied, and after summing the resulting resolvable pulse rates for each bin, an efficiency for photon counting can be defined as

$$\epsilon = \frac{\sum_{i=1}^{N} R_i'}{\sum_{i=1}^{N} R_i}. \tag{11}$$

In practice, count rates were kept low enough that corrections were <10%, corresponding to ~1 photon/sec at 400 mTorr of O_2. Selected correction factors, ϵ^{-1}, are shown on Fig. 14 for τ = 18 nsec and k_Q = 1.8 x 10^{-10} cm^3 $molecule^{-1}$ sec^{-1}.

The system as used for this work demonstrated a sensitivity for detecting NO(v=0) and NO(v=1) of better than 10^7 molecules/cm^3. This was measured directly, by titrating into the flowtube carefully prepared dilute solutions of NO in Ar, and this establishes an upper bound to the sensitivity of the system. Because the system as configured was appropriate for the kinetic studies performed, no attempt was made to further optimize the fluorescence collection system.

4. Data Acquisition Techniques

The calculated LIF γ- Band spectra for $0 \leq v \leq 7$, Figures 3-10, are sufficiently indentifiable that locating a particular structure for LIF studies was straightforward. The 4 bandheads are unmistakable for most levels, even in a relatively rapid wavelength scan of a band. Indeed, the rate at which very careful measurements of a spectral feature were made was so slow that scans such as that given in Fig. 15, in which count rates and coadded laser shots and wavelength scan steps were appropriate to making an accurate scan, took 3 to 5 hours to generate. Hence, wherever possible, rapid position-defining scans were made to locate a structure, usually a band head, and then scans over a limited part of the structure were made. Typically a scan from the LIF signal baseline at the long wavelength side of a bandhead was chosen as a start, and a scan made in .001 nm steps over the head and next 1 to 2 lines.

The signal obtained from such a scan has 4 components: (1) laser induced fluorescence from NO(v) or some other excited molecules, S_1; (2) afterglow background radiation, S_2; (3) scattered laser radiation seen by the phototube,

S_3; and, (4), electromagnetic pickup from the laser or other sources, manifesting itself as counts on the system, S_4. Every measurement was performed so as to define all these elements: A beam in, afterglow on measurement was made to get $I_1 = S_1 + S_2 + S_3 + S_4$; a beam in, no afterglow measurement gave $I_2 = S_3 + S_4$; an afterglow on, beam off measurement gave $I_3 = S_2 + S_4$; and a beam off, afterglow off measurement gave $I_4 = S_4$. The number of LIF counts for a measurement, F, is thus

$$F = I_1 - I_2 - I_3 + I_4 \pm \sqrt{I_1} \pm \sqrt{I_2} \pm \sqrt{I_3} \pm \sqrt{I_4}. \quad (12)$$

For typical data acquisition runs, F was the sum of components I_1 to I_4, each gathered by counting 1000 to 5000 laser shots. The laser power measurement was similarly acquired in digital form, so for the same number of laser shots, the laser power was given by

$$P = p \pm \sqrt{p}, \quad (13)$$

where p = the total number of counts from the laser power measuring system over the appropriate interval. The measure of LIF normalized by the laser power was used throughout this work as the experimentally measured result to be related to NO(v) concentrations. For brevity, this will be denoted ϕ, where

$$\phi = F/P. \quad (14)$$

The error bars shown in Figures 16-23 are the statistical counting error limits arising from the root terms in F and P. Counting times and conditions were chosen to minimize such terms, and the 400 mTorr ratioing work was performed routinely with the uncertainty in ϕ held to ±10% or less.

A fifth type of measurement was made routinely for all studies where any residual background signal was found: A spectral scan over the structure used to get ϕ was made with no O_2 in the system. Air leaks or residual O_2 in the N_2 or Ar would result in a background signal with a ϕ value which had be removed from the ϕ's measured with O_2 in the system. Baseline corrections of a few percent were actually required only for v=0. Spectral scans of this background indicated that they indeed were NO $\gamma(0,0)$ emission. These low level signals presumably resulted from small amounts of O_2 in the argon and nitrogen, and appeared to have a cumulative effect as O_2 was added throughout the day.

The production of NO in a specific vibrational level was observed as a function of O_2 partial pressure by measuring ϕ's at a standard O_2 pressure, chosen arbitrarily to be 400 mTorr for this study, changing the proportions of O_2 and Ar, measuring ϕ at this O_2 partial pressure, then returning to the standard 400 mTorr conditions and once more measuring ϕ. The resulting ratio of ϕ (P) to ϕ (400 mTorr) could thus be compared to ratios at other partial pressures of O_2 obtained at other times, since factors such as instrument gains, which could be expected to change or drift, cancelled out in the ratioing. This process of measuring ϕ ratios as a function of O_2 provided only a part of the information required to get relative NO(v) populations. Also essential was the ratio between one vibrational level and another at an appropriate O_2 partial pressure, and a measure of how much ϕ is reduced by O_2 through the quenching process

$$NO(A,v=0) + O_2 \xrightarrow{k_{15}} NO(x) + O_2^*, \qquad (15)$$

which impacts the fluorescence efficiency of the LIF technique.

All ratios between different vibrational levels were determined at 400 mTorr. In addition, all levels > 0 were ratioed to v=0. This was done to prevent compounding of errors that would occur if different vibrational states were used. The procedure was to determine at 400 mTorr the ϕ at level v, by scanning over a spectral structure, then changing the dye in the laser and if necessary, changing the doubling crystal, adding or removing filters with known transmittances over the laser power measuring photodiode, then measuring ϕ at v=0 for 400 mTorr. The procedure could be accomplished in ~1 hour, so it was possible to repeat it in a time period during which neither flow conditions nor instruments changed appreciably. The filters used on the photodiode were chosen so the power measuring system gains were unchanged from one vibrational level to the other. Counting times and all other photon counting system parameters were likewise unchanged.

The fluorescence efficiency effect of O_2 on the LIF system was examined by putting a constant concentration of NO into the flowtube, with all of the gaseous components (Ar, N_2, O_2) present as in the reaction measurements, varying the proportions of Ar and O_2 from all Ar to all O_2, and recording the change in observed ϕ's of a $\gamma(0,0)$ or a $\gamma(0,1)$ structure. NO concentrations were kept low, typically 10^9 to 10^{12} molecules/cm^3, so signal levels would not saturate the counting system. System linearity checks were performed as in the reaction studies. The results are the required set of correction factors to be applied to the reaction ϕ ratio data. The quenching rate coefficients for O_2 electronic quenching of NO(A) can be derived from the data, but the delayed-window counting system necessitates that the counting system parameters be entered into the analysis to get k_{15}. The results of these measurements and the analysis techniques used are described in following sections.

Another consideration in the technique of LIF was whether the polarization of the laser beam used for detection of NO(v) had an effect on the value of ϕ measured for a given pressure. Studies of NO($v \leq 1$) showed no effect of polarization on ϕ. Thus the polarization used for these studies was determined by the dye laser grating order used. For NO($v \geq 2$), measurements were made only on the polarization for which the laser produced the maximum amount of UV light.

III. Results

1. ϕ Variation as a Function of O_2 Partial Pressure

The most direct way to obtain the distribution of NO vibrational states produced by reaction (1), which may approximate the nascent distribution, is observation of NO(v) produced at O_2 partial pressures sufficiently low that the O_2 quenching of NO(v) is a minimal effect. The O_2 quenching rates k_2^v are known imprecisely, so the appropriate O_2 partial pressure for this work was also not well known. In this study, the O_2 partial pressure was varied from ~10 mTorr up to 400 mTorr for the measurements of NO(v) LIF signals. This range was sufficient to cover the transition zone from the low pressure end where O_2 quenching was insignificant to the high pressure end where O_2 quenching was effective in modifying NO(v) distributions; also, the low pressures were still high enough to minimize NO(v) production by the reaction of metastable N atoms with O_2. The data thus obtained were proportional to the concentration of NO(v) modified by fluorescence efficiency and count pile-up factors, as discussed earlier.

The full set of NO(v) LIF signals, corrected for fluorescence efficiency, is listed in Table 4. These data were all obtained at a constant mean flowtube pressure of 3.4 Torr, with the partial pressure of N_2 and the N atom concentration held constant.

The variation of ϕ as a function of O_2 partial pressure was studied using both the $^2\Pi_{1/2}$ and $^2\Pi_{3/2}$ states for those vibrational levels with LIF signals sufficiently large to permit measurement in reasonable amounts of time. The pressure dependences observed are given in Figures 16-23, and are corrected for quenching by O_2 of the fluorescing state, to be described later. At pressures less than about 50 mTorr, there is a linear dependence of NO(v) concentration on O_2 pressure, as shown by the linear dependence of ϕ on O_2 in the figures. At

higher pressures, where vibrational quenching by O and O_2 can become significant, the concentrations of NO(v) observed are lower than the extrapolation of the low pressure line.

It should be noted that even the NO(v=0) production (Fig. 16) departs from the extrapolated line. This is a behavior not predicted by a simple kinetic model and will be discussed at length in a subsequent section. The linear low-pressure behavior, however, taken with ratios of states to relate the 8 pressure dependence curves to each other, provide the information required to derive the low pressure NO(v) distribution.

Both spin states of NO($x^2\Pi$) were probed for levels $0 \leq v \leq 3$, in order to demonstrate that their dependence upon O_2 partial pressure was the same. No significant differences were observed, as seen in Figures 16-23. Since the spin states were observed to be in thermal equilibrium, as shown in Fig. 6, at high O_2 partial pressures, this behavior of ϕ with O_2 pressure implies that the spin states of the NO are in thermal equilibrium over the entire range of pressures with which we work.

The use of both spin states for measuring $\phi(O_2)$ was limited to $v \leq 3$, owing to the very long data acquisition times required for measuring ϕ for levels >3. Every point on Figures 16-23 represents a scan over a spectral structure, usually one of the 4 distinct bandheads. Typical scans were ~ .05 nm long at 1000 shots per .001 nm step and 10 shots/sec. Thus a typical data point on Figures 16-23 represents several hours of acquisition time, including 400 mTorr normalizing runs before and after the measurement. All points used were obtained this way, and this time factor represented a significant constraint on the types and quantities of data acquired. Individual figures thus are composed of points measured on several different days, all normalized to the 400 mTorr signal levels of their specific days.

2. NO(v) Ratios

The ratios of NO(v=0) to NO($1 \leq v \leq 7$) were obtained at 400 mTorr O_2 partial pressure by the techniques described in Section II. These ratios, which are listed in Table 5, represent the NO vibrational distribution at 400 mTorr of O_2 under our specific conditions. The distribution is indisputably the result of at least O_2 quenching of nascent NO(v) production. These ratios determine how the data of Figures 16-23 scale relative to each other.

The low pressure NO vibrational distribution obtained by scaling Figures 16-23 to the 400 mTorr ratios is given in Table 5 and plotted in Figure 24. If this low pressure distribution is in fact the nascent NO(v) production distribution, then the set of rate coefficients k_1^v is determined, using the overall value $k_1 = \sum_{v=0}^{7} k_1^v = .9E\text{-}16$ cm^3 $molecule^{-1}$ sec^{-1} from reference [1].

The extent to which the low pressure ratios approximate the nascent ratios depends upon factors such as N atom and O_2 quenching of NO(v) and thermal equilibrium in the molecule interrogated by LIF. Also, the relationship between $\phi(v)$ and NO(v) requires knowledge of the effects of O_2 on the fluorescing state, even though this need not be known to get ratios, so long as the linear behavior of ϕ on O_2 partial pressures at low pressures is not affected by such quenching. These concerns are addressed in subsequent sections.

3. Fluorescence Efficiencies

The rate coefficient for quenching of NO(A, v=0) by O_2 is known to be very large [36]. In order to properly assess the effect of this quenching on the high pressure measurements of $\phi(v)$, NO was added to the flow system with the discharge off, and the effect on the observed ϕ of changing the Ar/O_2 balance in the flowtube was explored. The variation in LIF signal thus observed relates rigorously to the difference in quenching rates for O_2 and Ar, but is

effectively just the O_2 rate, owing to the very low quenching rate coefficient, 6.3×10^{-14} cm^3 $molecule^{-1}$ sec^1, for Ar [37]. The quenching rate coefficient for deactivation of NO(A) by O atoms is unknown. At 400 mTorr O_2 partial pressure, the calculated concentration of atomic oxygen is $\sim 10^{12}$ atoms/cm^3; if the collisional deactivation probability for NO(A) quenching is ~ 1, the O atom quenching process has a characteristic time of ~ 1 m sec. Since only quenching processes which are significant on the time scale of the NO(A,V) radiative lifetime, 200 nsec, can change the fluorescence efficiency appreciably, we conclude that O atoms cannot change the value of ϕ over the range O_2 pressures in this work.

Fig. 25 shows the change in ϕ which occurs when O_2 is added to the flow tube. At .4 Torr, this change is seen to give an adjustment factor of 1.6 to 1.7 for relating ϕ to the actual concentration of NO.

The adjustment factor is related to the O_2 quenching rate coefficient, k_{15}, the radiative decay rate of NO(A,v=0), k_r, and the counting system window opening and closing times measured from the laser pulse, t_1 and t_2, by the equation

$$\frac{\phi(O_2)}{\phi(0)} = \frac{k_R}{k_s} * \frac{\left(e^{-k_s t_2} - e^{-k_s t_1}\right)}{\left(e^{-k_R t_2} - e^{-k_R t_1}\right)} , \qquad (18)$$

where $\phi(O_2)$ is the signal with O_2 present, $\phi(0)$ is the signal with no O_2 in the flowtube, and $k_s = k_R + k_{15} * [O_2]$.

The radiative lifetime of NO(A, v=0) is well established at 200±10 nsec [20], with older references ranging from 175±10 nsec to 220±2 nsec [38]. k_{15} was measured previously by Campbell and Mason [36] as the ratio k_{15}/k_R, which they report to be $(5.3 \pm .7) \times 10^{-17}$ cm^3/molecule (units converted). Taking $k_R = 5. \times 10^6$ sec^{-1}, one obtains $2.3 \times 10^{-10} < k_{15} < 2.9 \times 10^{-10}$ cm^3 $molecule^{-1}$

sec^{-1}. The value of k_{15} derived in this work is appropriate for radiative efficiency corrections in this work, as it contains all the systematic biases of the specific experiment. There is no reason to believe it represents an absolute value of k_{15} more accurate than that value reported in ref. [36].

The fluorescence efficiency data presented in Fig. 25, when reduced using Eq. (18), lead to a value of k_{15} of $1.5 \times 10^{-10} \leq k_{15} \leq 2.1 \times 10^{-10}$ cm^3 $molecule^{-1}$ sec^{-1}. All fluorescence efficiency adjustments used in Figures 16-22 were calculated using $k_{15} = 1.8 \times 10^{-10}$ cm^3 $molecule^{-1}$ sec^{-1}. Fig. 25 presents the correction factors applied for the O_2 partial pressure range of 10 to 400 mTorr. Also shown in this table are the correction factors resulting from applying $k_{15} = 2.6 \times 10^{-10}$ cm^3 $molecule^{-1}$ sec^{-1}, within the range derived from Ref. [36], as an indication of the dependence of the correction factor on k_{15}.

It should be emphasized that the fluorescence efficiency factor is required to relate the shape of the LIF signal vs O_2 pressure curve to real NO(v) concentrations, but that at any given pressure, relative population ratios for NO(v) levels are known, even if k_{15} is not known, simply because all of the LIF work has been performed by exciting NO(x,v) to NO(A,v=0). Further, at low O_2 pressures even the shape of the curves in Figures 16-23 is independent of the value of k_{15} assumed, since there simply is not enough O_2 available for a significant reduction in fluorescence efficiency.

4. Thermal Equilibrium Studies

The calculated LIF spectra of Figures 3 to 10 are based on the assumption of rotational and spin-state thermal equilibrium at 300°K. Careful scans were made of NO(v<0) LIF spectra in order to verify the validity of such assumptions. The NO(v) studied was produced by reaction (1). In the case of NO(v=0) and NO(v=1), NO from a constant low concentration source of pure NO mixed with the normal undischarged flowtube species was also studied, as this

was certain to be in thermal equilibrium. This provided a direct check of the calculations.

The NO LIF spectra thus obtained appear to agree with the calculated γ Bands. This behavior had to be demonstrated, since the O_2 quenching process represented by k_{15} could conceivably have a J-state or spin-state dependence. The observation of thermal-appearing LIF spectra does not actually rule this out; we merely note that at the total flow tube pressure of 3.4 Torr used for all work described here, and for an O_2 partial pressure range of < 100 mTorr up to 400 mTorr, had the profile of a thermal excitation spectrum. This greatly simplifies the interpretation of fluorescence data and is reasonable, based upon the large number of collisions an NO molecule undergoes in its 1 msec lifetime in the flowtube.

The assumption of thermal equilibrium is also consistent with the observation that the flowtube wall temperature, measured using a type K thermocouple outside the tube, remained at room temperature throughout day-long sessions of operation. If all of the energy of the reaction were in fact applied to heating the gas, a gas temperature rise of < 4°K would occur in this system. This is important in keeping the overall rate of reaction (1) a constant. The temperature dependence of k_1 is given by [39]

$$k_1(T) = (3.3E\text{-}12)e^{-3150./T}. \qquad (19)$$

This specifies that a change in k_1 of ~ 4% occurs per °K, around room temperature. Since the uncertainty of k_1 quoted in reference [39] is 33% at 300°K, variations in k_1 due to thermal drift of the system were assumed to be insignificant.

At vibrational levels >1, where no thermal room-temperature population of NO(v) could be produced in concentrations sufficient for detection with our system, spectral structures were compared to calculations and within error limits of ~±10% were consistent with a calculated 300°K rotational distribution. Furthermore, the NO γ Bands are configured so that with the spectral resolution of our laser, the structures which appear to be one spectral line are in the majority of cases nearly coincident lines, one with a low rotational quantum number and one with a high rotational quantum number. Thus, the appearance of the LIF γ-Band spectrum is only weakly a function of temperature.

The agreement between the 300°K calculations and our observations is shown in Table 6, where the spin state ratios are compared, and, less well, in Fig. 15, in which the agreement between calculated and observed structure of γ(0,3) is shown on a 400 mTorr O_2 partial pressure spectrum resulting from probing the flowtube in which the $N + O_2$ reaction was occurring.

5. Absolute Value of NO(v=1) in the Flowtube

This paper presents the low O_2 pressure distribution of NO(v) produced by reaction (1), determined by ratioing curves of $\phi(v)$ vs O_2 pressure to get apparent nascent ratios and alloting vibrational reaction rate coefficients k_1^v so that $\sum_{v=0}^{7} k_1^v = k_1$, where k_1 is the well-known overall reaction rate coefficient of reaction (1) [1]. An alternate method of measuring k_1^v is to add into the flowtube known amounts of NO in that vibrational level and calibrate the system for converting ϕ into [NO(v)]. This technique is impractical for most vibrational levels, but simple for v=1, which exists in thermal equilibrium in room temperature NO in concentrations within the dynamic range of our system, when NO is titrated into the system in quantities which will not effect the fluorescence efficiency of the LIF system.

A measurement of the absolute concentration of NO(v=1) produced by the N + O_2 reaction under our standard flow conditions was made by matching the signal from the reaction with NO titrated into the same gas mixture in the flowtube, but with the discharge off. The results of this exercise, using purified NO and the titration system described previously, was that

$$[NO(v=1)] = 6.65 \times 10^7 \text{ molecules/cm}^3,$$

for 30 mTorr of O_2. Solving the steady state relationship, equation (4), for k_1^1, one obtains

$$k_1^1 = k_3 \frac{[NO(v=1)]}{[O_2]} = 2.3\text{E-}18 \text{ cm}^3 \text{ molecule}^{-1}\text{sec}^{-1},$$

which compares favorably with the value of 3.8E-18 cm^3 $molecule^{-1}$ sec^{-1} obtained by ratioing vibrational levels. This agreement is an excellent indication of the validity of the rate coefficients, k_1^v, reported in this work.

IV. Discussion

1. Appropriate Kinetic Models

Most flowtube studies are performed under conditions in which extraneous kinetic processes must be tolerated. All studies of the $N(^4S) + O_2$ reaction, the IR chemiluminescent work and the LIF work alike, have been performed under complex kinetic conditions. The purpose of this section is to describe the extent to which the best available kinetic model for the flowtube system reproduces the results given in Section III, if our low O_2 pressure NO(v) production rates are included in the model.

The NO(v) distribution observed in this work at low O_2 partial pressures can be interpreted to represent the nascent branching ratios of reaction (1), if certain assumptions are valid. These assumptions are important in the interpretation of the results from all studies of reaction (1), and in the validity of radiance modeling efforts, so they will be described in detail. The full kinetic model used for analysis of the data, given in Table 7, is based upon the assumption that all significant processes are identified and present in the model. The process

$$NO(v) + N \rightarrow NO(v'<v) + N, \qquad (19)$$

where v' may in fact be a distribution of product levels down to v=0, is omitted from Table 7 because no relevant studies of (28) have been performed. Our observed distribution of NO vibrational levels is predominantly in v=0, and the possibility exists that this is the result of very rapid N atom quenching. All studies of reaction (1) performed in this work had an N atom concentration of $2. \times 10^{13}$ atoms/cm^3, since lower concentrations allow O_2 quenching effects to predominate and higher concentrations resulted in an afterglow UV radiance which reduced the sensitivity of the LIF system. If the collisional deactivation

probability of NO(v) by N were ~1, process (19) would be ~6 times faster than removal of NO(v) by reaction with N atoms. Thus, process (19) could, in principal, be the dominant kinetic process in the flowtube, or in the integrating spheres used in IR chemiluminescent studies. Process (19) is insignificant in the CHOCHISE studies of $N^* + O_2$ [40] owing to the short retention times and low N atom concentrations in that system.

In order for our NO(v) distribution observed at low O_2 partial pressures to actually be the nascent distribution, the probability of NO(v) quenching by N atoms must be less than for removal of NO(v) by direct reaction with N atoms. If this is not so, the ratios presented here are not the nascent distribution, but still constitute a lower bound for the fraction of energy deposited in infrared-active NO states by reaction (1).

A surprisal analysis of reaction (1), performed using the techniques of ref. [41], is illustrated in Fig. 27. The prior distribution, denoted by P_o in the figure, was calculated on the assumption that the collision energy was 1.7 eV, the sum of the reaction exothermicity and the activation energy [1], and the approximate formulas for the final state distributions from Ref. [41]. The experimental distribution P_e is compared to P_o in the figure by the ratio P_o/P_e. Fig. 27 illustrates a break in the surprisal behavior between v=0 and v=1, which is suggestive of complication to the simple reaction mechanism assumed. This is consistent with idea that process (19) is in fact significant under our conditions. All subsequent kinetic descriptions of the system will omit this process, however, since no hard data exist for justifying its inclusion.

In fact, the surprisal plot for the $N^* + O_2$ study made by Kennealy et. al. [40], which covers the range $1 \leq V \leq 7$, shows a large surprisal factor for V=1 production under conditions where N atom quenching of NO(v) was insignificant.

The possibility exists that for both $N(^4S) + O_2$ and $N^* + O_2$, NO(v=0) is a significant direct product of the reactions.

The most simple kinetic analysis of the $N(^4S) + O_2$ and $N(^4S) + NO$ system, the steady state solution

$$[NO(v)]_{ss} = \frac{k_1^v}{k_3} [O_2], \qquad (4)$$

represents only the creation and N atom removal loss terms for NO(v). Terms arising from O_2 quenching, for instance, significantly change the distribution of NO(v) at O_2 partial pressures above 50 to 100 mTorr. The set of O_2 quenching rates reported by Caledonia [15] is plotted in Fig. 28; it is clear that at O_2 partial pressures of a few hundred mTorr, O_2 significantly alters the distribution of NO vibrational levels observed in the system and invalidates eq. (4).

The full set of relevant reactions identified for inclusion in the Aerospace Corp. N-Element Chemistry System (NEST) computer code, used for all kinetic calculations described henceforth, is given in Table 7. Processes 1-3 are the only important processes identified for determining the NO vibrational distribution in our system, as indicated by the characteristic time, τ, listed in Table 7. Of negligible effect in our work are the other 24 processes listed in Table 7. Most reactions in that section are too slow to have an effect, since they must compete with the rapid processes 2 and 3. Some, such as the metastable N atom reactions with O_2, are so rapid that the $N(^2D)$ or $N(^2P)$ is used up and the NO(v) product is formed and destroyed long before the 30 msec reaction time of this work has elapsed. Some processes, such as quenching of NO(v) by O atoms, become significant at O_2 pressures > 400 mTorr, and must be considered in the analysis of most IR chemiluminescent data.

Careful analysis shows that both $N_2(A)$ and $N(^2P)$ have steady state concentrations in the flowtube which could be significant in this experiment. $N(^2P)$, produced by quenching of $N_2(A)$ by $N(^4S)$, reacts with O_2 to produce NO with an unknown absolute vibrational distribution. At 10 mTorr of O_2, this reaction can thus produce as much as 6% of the total NO in the system. This contribution drops very rapidly, so that at 50 mTorr of O_2, it is ~.1%. At our lowest pressures of O_2 this reaction could therefore add a bias, but the contribution is less than the statistical uncertainty associated with each measurement.

$N_2(A)$ could conceivably react directly with O_2 to produce NO in the system. This reaction has not been reported in the literature and is almost certainly not a principal path in the $N_2(A)$ - O_2 interaction; it is discussed here for completeness. The maximum contribution to this reaction could make to the NO in the flowtube ranges from ~8% at 10 mTorr of O_2 to ~4% at 50 mTorr; energy is available for populating vibrational levels for higher than 7. If production were in upper vibrational levels where reaction (1) is relatively unproductive, our measurements would be seriously in error. However, no infrared observations of NO chemiluminescence have delected levels >7 [8,9,10], even through the high concentrations of N and O_2 in those studies and the sensitivity of the sensors would have favored detection if the NO(v) was actually produced. $N_2(A) + O_2$ is thus of slight importance in this work.

The results of a typical NEST analysis performed using our values of k_1^v and the assumption that $k_3^v = k_3$ are given in Table 8. The values of k_2^v used for this calculation are listed in Table 9, and are the mean values reported in ref. [15], except for k_2^7, which was chosen to be the lower bound of ref. [9], based on the shape of the [NO(v=7)] vs O_2 pressure curve, Fig. 23. It is seen that the resulting NO(v) distribution at 50 mTorr is still approximately directly proportional to the formation rate coefficients, k_1^v, but that at 400 mTorr the

distribution has shifted heavily towards lower vibrational levels, due to quenching. It is also clear from calculations that no species exist in sufficient concentrations, besides N, O_2, and possibly O, to complicate the analysis, if the significant processes are actually limited to those in Table 7. To have an effect, a process must successfully compete with the N atom removal reaction, Eq. (3).

Comparison of calculated and observed NO(v) distributions can be made in two ways: (1) by examining the NO(v) ratios as functions of O_2 partial pressure; or (2) by examining the shapes of the corrected ϕ vs O_2 data, properly ratioed at 400 mTorr. Method (1) ratios away any needed fluorescence efficiency correction factors; method (2) is a complete test of how well the full kinetic scheme including quenching of NO(A, v=0), is understood.

Table 9 shows the results of calculating the NO(v) ratios using a set of O_2 quenching rate coefficients based on ref. [15]. It is clear that the agreement between experiment and these calculations is fair, the largest discrepancy occurring at v=7, indicating that the set of k_2^v values chosen appears to be approximately correct. If the values of k_2^v are varied for maximum ratio agreement at 400 mTorr, a set of slightly lower quenching rate coefficients and calculated ratios is defined, which is also listed in Table 9. We conclude that the kinetic model listed in Table 7, used with our best values of k_2^v reproduces our observed NO(v) ratios well.

If the shapes of the NO(v) vs O_2 curves shown in Figs. 16 to 23 are compared to the curves based on our best kinetic model, we find that there is no way to produce agreement. The basic problem is exemplified by the NO(v=0) data of Fig. 16. Based on any first order kinetic model for NO(v) production, [NO(v=0)] must be directly proportional to $[O_2]$ or must increase more rapidly than the direct proportion as NO(v) is quenched to NO(v=0) by the O_2. The

observed O_2 pressure dependence, an apparent decreasing efficiency of NO(v=0) production with increasing O_2 pressure, cannot be modeled by varying any of the rates coefficients for the processes in Table 7, or even by changing the nature of the quenching process NO(v) + O_2 to allow $\Delta v>1$ to occur. The extent of this problem, which may occur to some extent for all the vibrational levels, is illustrated in Figure 29 which shows data for the v=0 level.

Three distinct types of reasons for the discrepancy between observation and calculation can be postulated: (1) that the high O_2 pressure data are simply wrong; (2) that an NO(A) quenching process has been overlooked or underrated; or (3), that there is a fundamental flaw in the kinetic model. These categories will be addressed individually.

There is, of course, no way to totally exclude the possibility that the high O_2 pressure data are simply wrong. However, extreme care has been taken to avoid such systematic errors as counting system pulse pileups, line center absorption or saturation, background signal shifts, and the like, as described in Section II. The outward appearance of thermal rotational- and spin-state equilibrium has been demonstrated, as has the absence of any LIF signal due to overlapping γ- or β-bands or other molecular species. These requirements are essential for establishing the validity of the vibrational state ratio data and do so beyond a reasonable doubt. Matching the data of Figures 16-23, however, requires that the fluorescence efficiency factors be correct as well.

Increasing the fluorescence efficiency correction to that calculated for $k_{15} = 5. \times 10^{-10}$ cm^3 molecule^{-1} sec^{-1} is sufficient to match the calculated variations of NO(v) populations as function of O_2 partial pressure to the observations. There is no justification for accepting such a high value of k_{15}, however. The fluorescence efficiency correction factor was measured directly, as described in Section III, in an undischarged flow system having the N_2, O_2,

and Ar mixtures used for the LIF work. k_{15} was found to be 1.8×10^{-10} cm^{-3} $molecule^{-1}$ sec^{-1} from this experiment, and whatever systematic errors are present in this measurement were similarly present in all our other work. A careful examination of the efficiency correction factor of Fig. 26 thus did not identify the source of the discrepancy.

A flowtube constituent present only when the discharge is on could easily add a second quenching mechanism for deactivating NO(A,v=0). However, in order to be competitive with the NO(A,v=0) radiative lifetime and the O_2 quenching process, the concentration of such a quenchant would have to be ~.2 Torr or larger. Table 8 shows no species resulting from the reactions to be remotely close to this level. Thus we lack a mechanism for increasing the fluorescence efficiency correction factors.

Since our set of k_1^v values is derived from ratios of signals at the same O_2 pressure, efficiency correction changes do not change the ratios we report. The effect of changing k_{15} to reproduce the shape of the ϕ vs O_2 curves of Figures 16-23 was studied; Fig. 29 shows the difference between the v=0 data corrected using $k_{15} = 1.8 \times 10^{-10}$ cm^3 $molecule^{-1}$ sec^{-1} and $k_{15} = 5. \times 10^{-10}$ cm^3 $molecule^{-1}$ sec^{-1}. The high value produces a close match between observation and NO(v=0) populations calculated using our set of k_1^v values; other vibrational levels show a similar match in shape. There is no experimental justification for applying this correction factor, however, and the set of k_1^v values derived from the experimental data is independent of k_{15}.

The final possibility, that the kinetic model is somehow wrong, can be divided into the postulate that there is a product that removes NO(v=0) in competition with N atoms and the postulate that reaction (1) is somehow not a simple first-order reaction. Both ideas can be shown to be adequate for explaining the shape of the corrected ϕ vs O_2 data, but neither appears to have

much credibility. The first postulate, that there is another NO removing atom or molecule in the system, requires that the concentrations of that unknown species be ~ 10^{12} cm^{-3}. The modeled flowtube composition shows no likely candidate for this reaction at 400 mTorr of O_2. The most significant objection to the second explanation is that other studies [6,7] have concluded that k_1 and k_3 are adequately represented by a simple first-order model, for O_2 partial pressures as high as a few Torr.

No explanation can be offered at present for the behavior of the corrected ϕ values as functions of O_2 pressure. It must be emphasized that this mystery exists at high pressures only and in no way effects the validity of the NO(v) ratio measurements at any pressure.

2. Comparisons with Other Studies

The two previous studies of reaction (1) in which NO vibrational distributions were measured [9,10], were performed using first overtone IR chemiluminescence; thus only data on NO($v > 2$) production were obtained. The results of these studies, together with the low pressure and 400 mTorr distributions reported in this work, are presented in Table 10.

Agreement between the IR values is seen to be good; both define a generally decreasing dependence of NO(v) on increasing v. The LIF study at 400 mTorr O_2 partial pressure demonstrates a much weaker dependence of NO(v) on v.

An examination of the relative importance of the various kinetic processes in the different experiments, all of which have different O_2 concentrations, N atom concentrations, reaction times, and resulting O atom concentrations, reveals that a simple direct comparion of the reported NO vibrational distributions cannot be made. Table 11 lists the important differences between the experiments. It is seen that only the low O_2 pressure work reported here is clearly dominated by the N atom removal process, (3). The high pressure LIF

work reported here and the IR work of Whitson et. al. [9], are highly dominated by O_2 vibrational quenching of NO(v), process (2). The work of Rahbee and Gibson [10], shown here for 400 mTorr but actually ranging from 200 mTorr to 600 mTorr, is reasonably free of O_2 quenching effects, but probably subject to heavy quenching of NO(v) by O atoms, process (4), if the reaction rate coefficient for quenching of NO(v>1) is as fast or faster than the value 6.5×10^{-11} cm^3 $molecule^{-1}$ sec^{-1} reported by Fernando and Smith for v=1 [17].

Unfortunately, the details of the quenching process

$$NO(v) + O \overset{k_{20}}{\rightarrow} NO(v') + O \qquad (20)$$

are unknown. A model which assumes a constant k_{20} and that v' = 0, does not fit the various observations, since the quenching does not alter relative NO(v > 2) ratios. A model which assumes $\Delta v=1$ fits the observed data more closely, but too many rate coefficients and process details are lacking for the model to have significance.

Rahbee and Gibson [10] present two sets of rate coefficients for k_1^v where $2 \leq v \leq 7$. One set is calculated using a kinetic model including O_2 quenching of NO(v), but no quenching by O atoms; the other set includes O atom quenching, assuming that k_{20}^v is independent of v. The two sets of results, both listed in Table 10, are considerably different. The set including O atom effects shows increased population in the higher vibrational levels, but does not approach the low pressure distribution reported here. This is not surprising, since process (20) is too poorly characterized to allow proper kinetic handling.

The work by Whitson et. al. [9] totally omitted process (20) in its analysis, but this was an omission based on kinetic grounds. The concentration

of O atoms in that work was sufficiently low that this was an appropriate simplification. The problem in the data analysis of that study is simply the extensive modeling required to convert measurements made at 3 Torr of O_2 to nascent ratios.

We conclude that no reasonable comparison of the previously reported nascent $v \geq 2$ ratios can be made with each other or this work, and that it is unlikely that the calculated nascent ratios of references [9] or [10] are correct. There is no basis for distrusting any of the previous IR chemiluminescence measurements, even though they vary considerably from this work, as seen in Table 10. All of the measurements made at high O_2 pressures should show an NO(v) distribution skewed towards low v, and they do. This is shown in Fig. 30. Unfortunately the processes leading to these distributions are understood too poorly to be modeled.

3. Implications of This Work for Atmospheric Radiance Models

If the rate coefficient for the N + NO reaction is not a function of v, the NO vibrational distribution reported here for low O_2 partial pressures is in fact either the nascent distribution from reaction (1) or a distribution shifted towards lower mean vibrational energy by N atom quenching of NO(v). Reaction (1) is then seen to deposit 29% of its available 1.29 eV reaction exothermicity into vibrational excitation of the NO to level ≥ 1, and 28% into levels ≥ 2. This is ~ 3 times more energy than predicted by Rahbee and Gibson [10] based on an earlier work by Hushfar et al. [42]. Furthermore, 42% of the NO(v) molecules are produced in levels > 0, and 38% in levels > 1. Thus, reaction (1) is significantly more efficient in producing IR radiation than was previously believed, and may in fact be even more efficient than these measurements indicate.

A shift upwards in the mean vibrational level can translate into large increases in photon production under some conditions, since $A_{\Delta v=1}$ and $A_{\Delta v=2}$ both increase rapidly with v, as shown in Table 12. For instance, in a IBC Type I Aurora at 100 km, with [O] = 2.2 x $10^{11}/cm^3$ [43], the radiative lifetime of NO(v=1) is = 144 msec, which is slow compared to the characteristic time of O atom quenching, τ_o = 69 msec, resulting in a photon production efficiency for NO(v=1) which is lower than for NO(v>1) levels. Table 13 lists auroral atmospheric parameters for altitudes from 85 to 160 km [43]; it is obvious from this that the processes for NO(v) quenched by O and O_2 must be known in order to successfully model disturbed atmospheres in this region. It is also clear that N atom quenching of the NO(v) is of no consequence under these conditions, so a profound difference between upper atmospheric NO vibrational distributions and those produced in laboratory experiments could exist.

A nascent distribution of the NO(v) product of reaction (1) has been reported, based for the first time on direct observation of all 8 NO vibrational levels involved. The validity of this nascent distribution hinges on two assumptions involving N atoms, both of which are of crucial importance in the modeling of atmospheric phenomena and in the interpretation of laboratory studies. These processes are: (1), the quenching effects of N atoms on NO(v), which has not been studied; and (2), the destruction of NO(v) by N, which is assumed to be constant for $0 \leq v \leq 7$.

V. Conclusions and Recommendations

The results of this work can be separated into three categories: (1) the development and demonstration of an experimental technique for NO studies; (2) the measurement of NO(v) population ratios in a flowing afterglow experiment; and (3) the identification of processes of potential importance which must be understood before the results of this work or of infrared radiance models can be accepted without reservation.

This work describes the first study of vibrationally excited NO performed using the technique of laser induced fluorescence detection. The feasibility of using this technique for probing NO(v) concentrations at least as low as 10^7 molecules/cm^3 has been established, and a significant step towards the detailed understanding of the $N(^4S) + O_2$ reaction has been taken. It is clear that LIF detection of NO(v) can become a powerful experimental technique under conditions where the NO(A,v) excited state is not heavily quenched.

The low pressure distributions reported here must be accepted, with the caveats mentioned throughout this work, to define a lower bound of reaction infrared-active state production, since it is likely that the unknown N atom effects, if real, tend to lower the degree of product vibrational excitation. Thus this study has established that the $N(^4S) + O_2$ reaction deposits at least 3 times more energy into infrared active states than was previously believed.

Finally, the process of quenching of NO(v) by O was identified as the probable source of a significant vibrational distribution perturbation in some prior studies of the $N(^4S) + O_2$ reaction. No information regarding the rate coefficient for NO(v>1) exists, and it too, is potentially an important atmospheric process involved in determining the vibrational distribution in the disturbed atmosphere.

We recommend that these processes,

$$N + NO(v) \rightarrow N + NO(v'),$$

$$N + NO(v) \rightarrow N_2 + O,$$

$$O + NO(v) \rightarrow O + NO(v'),$$

be the subjects of further experimental work, and that the results of the work reported here be scrutinized in the light of those new studies.

VI. References

1. V. N. Kondratiev, Rate Constants of Gas Phase Reactions, English translation, ed. R. M. Fristom (National Bureau of Standards, Washington, D. C., 1972).
2. P. A. Benioff, G. Das, and A. C. Wahl, J. Chem. Phys. 67, 2449 (1977).
3. G. Das and P. A. Benioff, Chem. Phys. Lett. 75, 519 (1980).
4. C. W. Wilson, Jr., J. Chem. Phys. 62, 4842 (1975).
5. G. B. Kistiakowsky and G. G. Volpi, J. Chem. Phys. 27, 1141 (1957).
6. M. A. A. Clyne and B. A. Thrush, Proc. Roy. Soc. A261, 259 (1961).
7. J. D. Clark and J. P. Wayne, Proc. Roy. Soc. A316, 539 (1970).
8. F. Hushfar, J. W. Rogers, and A. T. Stair, Jr., Appl. Opt. 10, 1843 (1971).
9. M. E. Whitson, Jr., L. A. Darnton, and R. J. McNeal, Chem. Phys. Lett. 41, 552 (1976).
10. A. Rahbee and J. J. Gibson, J. Chem. Phys. 74, 5143 (1981).
11. R. E. Murphy, E. T. P. Lee, and A. M. Hart, J. Chem. Phys. 63, 2919 (1975) 2919.
12. R. P. Fernando and I. W. M. Smith, J. Chem. Soc. Farad. Trans. II 77, 459 (1981).
13. J. C. Stephenson and S. M. Freund, J. Chem. Phys. 65, 4303 (1976).
14. J. Kosanetzky, U. List, W. Urban, and H. Vormann, Chem. Phys. 50, 361 (1980).
15. G. Caledonia, private communication.

16. See D. L. Balch, D. D. Drysdale, D. G. Home, and A. C. Lloyd, Evaluated Kinetic Data for High Temperature Reactions, Volume 2, Butterworths, London, 1973, for a review of the N + NO reaction. The value of k_3 used is taken from J. H. Lee, J. V. Michael, W. A. Payne, and L. J. Stief, J. Chem. Phys. 69, 3069 (1978).

17. R. P. Fernando and I. W. M. Smith, Chem. Phys. Lett. 66, 218 (1979).

18. K. Glanzer and J. Troe, J. Chem. Phys. 63, 4352 (1975).

19. See, for example, R. Freedman and R. W. Nicholls, J. Molec. Spect. 83, 223 (1980) and the references therein.

20. G. R. Mohlman, H. A. Van Sprang, E. Bloeman, and F. J. DeHeer, Chem. Phys. 32, 239 (1978).

21. D. J. Flinn, R. J. Spindler, S. Fifer, and M. Kelly, J. Quant. Spec. Rad. Trans. 4, 271 (1964).

22. R. Engleman, Jr., and P. E. Rouse, J. Molec. Spec. 37, 240 (1971).

23. J. B. Tatum, Ap. J. Suppl. Ser No. 124 (1967).

24. A Schultz, H. W. Cruse, and R. N. Zare, J. Chem. Phys. 57, 1354 (1972).

25. A. Schadee, B. A. N. 17, 341 (1964).

26. A. Schadee, Astron. and Astrophys. 14, 401 (1971).

27. J. A. Meyer, D. W. Stetser, and W. G. Clark, J. Phys. Chem. 76, 1 (1972).

28. D. Husain, S. K. Mitra, and A. N. Young, J. Chem. Soc. Faraday Trans. II 70, 1721 (1974).

29. W. Brennan, R. V. Gutowski, and E. C. Shane, Chem. Phys. Lett. 27, 138 (1974).

30. J. Kosenetzky, U. List, W. Orban, and H. Vormann, Chem. Phys. 50, 361 (1980).

31. M. E. Whitson, Jr. and R. J. McNeal, J. Chem. Phys. 66 2696 (1977).

32. R. L. Taylor and S. Bitterman, Rev. Mod. Phys. 41, 26 (1969).

33. F. Kaufman and J. R. Kelso, Proc. 7th Int. Symp. Combustion, 53 (1958).

34. H. S. Judeikis, J. Phys. Chem. 84, 2481 (1980).

35. J. D. Ingle, Jr., and S. R. Crouch, Anal. Chem. 44, 777 (1972).

36. I. M. Campbell and R. S. Mason, J. Photochem. 8, 321 (1978).

37. H. P. Broida and T. Carrington, J. Chem. Phys. 38, 136 (1963).

38. See, for example, A. J. Smith and F. H. Read, J. Phys. B.: Atom. Molec. Phys. 11, 3263 (1978).

39. R. F. Hampson and D. Garvin, Natl. Bur. Stads. Rept. NBS-TN-866 (1975).

40. J. P. Kennealy, F. P. DelGreco, G. E. Caledonia, and B. D. Green, J. Chem. Phys. 69, 1574 (1978).

41. R. D. Levine and R. B. Bernstein, Acct. Chem. Res. 7, 393 (1974).

42. F. Hushfar, J. W. Rogers, and A. T. Stair, Jr., Appl. Opt. 11, 1656 (1972).

43. A. G. Hurd, J. W. Carpenter, T. C. Degges, W. F. Grieder, W. P. Reidy, O. Shepherd, A. T. Stair, Jr., R. R. O'Neal, J. C. Ulwick, D. J. Baker, and K. D. Baker, Comparison of Icecap and Excede Rocket Measurements with Computer Code Predictions, Report AFGL-TR-77-0060, Air Force Geophysics Laboratory, Hanscom AFB, Mass., 1977.

44. R. W. B. Pearse and A. G. Gaydon, The Identification of Molecular Spectra, 4th Edition, John Wiley and Sons, New York, 1976.

45. J. C. Stephenson, J. Chem. Phys. 59, 1523 (1973).

46. H. Horiguchi, S. Tisirchiza, Japanese J. Appl. Phys. 18, 1207 (1979).

47. R. F. Hampson, Chemical Kinetic and Photochemical Data Sheets for Atmospheric Reactions, U.S. Dept. of Transporatation Report FAA-EE-80-17, (1980).

48. L. J. Stief, W. A. Payne, J. H. Lee, and J. V. Michael, J. Chem. Phys. 70, 5241 (1979).

49. K. H. Becker, W. Groth, and D. Thran. Symp. Int. Combust. Proc. 14th, 353 (1973).

50. D. L. Balch, D. D. Drysdale, and D. G. Horne, Evaluated Kinetic Data for High Temperature Reactions, Vol. 2, Homogeneous Gas Phase Reactions of the H_2-N_2-O_2 System, Butterworths, London, 1973.

51. K. L. Demerjian, J. A. Kerr, and J. G. Calvert, Advances in Environmental Science and Technology, Vol. 4, Edited by J. N. Pitts and R. L. Metcalf, John Wiley, New York, 1974.

52. I. M. Campbell and C. N. Gray, Chem. Phys. Lett. 18, 607 (1973).

53. O. Klais, R. C. Anderson, M. J. Kurylo, Int. J. Chem. Kinetics 7, 469 (1980).

54. D. D. Davis, S. Fischer, and R. Schiff, J. Chem. Phys. 61, 2213 (1974).

55. O. J. Dunn and R. A. Young, Int. J. Chem. Kinetics 8, 161 (1976).

56. M. A. A. Clyne and I. S. McDermid J. Chem. Soc. Farad Trans. I 71, 2189 (1975).

57. G. Karl, P. Kruus, J. C. Polanyi, I. W. M. Smith, J. Chem. Phys. 46, 244 (1967).

58. F. R. Gilmore, J. Quant. Spec. Rad. Trans. 5, 369 (1965).

Table 1 Franck-Condon Factors and Approximate Wavelengths for selected NO γ-Bands

Band	FCF[25]	Wavelength (nm) [44]
0,0	.16535	226.28
3,4	.11305	228.41
2,3	.075234	230.95
0,1	.26359	236.33
1,3	.072141	244.0
0,2	.23764	247.71
2,5	.034327	251.64
1,4	.13492	255.0
0,3	.16044	258.75
2,6	.088484	263.07
1,5	.13391	267.14
0,4	.090708	271.32
2,7	.10565	275.52
1,6	.098577	280.08
0,5	.045562	284.98
1,7	.060770	294.19
0,6	.021077	299.76
0,7	.0091957	317.07

Table 2: Structure of the Small $^2\Pi_{3/2}$ Bandhead of the $\gamma(0,0)$ Band

λ(nm)	J	Relative Intensity
226.882	1.5	.32
226.885	19.5	.04
226.906	2.5	.36
226.910	18.5	.05
226.927	3.5	.39
226.931	17.5	.07
226.945	4.5	.41
226.948	16.5	.09
226.961	5.5	.41
226.964	15.5	.11
226.973	6.5	.41
226.976	14.5	.14
226.983	7.5	.39
226.985	13.5	.17
226.991	8.5	.36
226.992	12.5	.21
226.996	11.5	.25
226.997	10.5	.29

Table 3. Experimental Specifications for γ-Band Laser Induced Fluorescence Detection of NO(v ≤ 7)

TRANSITION (γ Band)	$^2\Pi_{1/2}$ Bandhead WAVELENGTH (nm)	DYE	DOUBLING CRYSTAL
0-0	226.3	Coumarin 460	KB5
0-1	236.3	Coumarin 480	KB5
0-2	247.1	Coumarin 500	Lithium Formate
0-3	258.8	Coumarin 500	Lithium Formate
0-4	271.3	Coumarin 540A	KDP
0-5	284.9	Rhodamine 590	KDP
0-6	299.8	Rhodamine 610	KDP
0-7	315.9	Rhodamine 640	KDP

Table 4. Experimental Data. ϕ^v as a function of O_2 partial pressure for v=0 through V=7. The values of ϕ^v are corrected for fluorescence efficiency, using the factors plotted in Fig. 26, derived from k_{15} 1.8E - 10 cm^3 molecule-1 sec^{-1}.

Table 4a. V=0

P(mTorr)	Corrected
18*	.15 < .16 < .17
28	.08 < .10 < .12
30*	.14 < .15 < .16
35	.17 < .19 < .21
41	.29 < .33 < .37
41	.29 < .33 < .37
55	.16 < .20 < .24
73*	.33 < .35 < .37
100	.40 < .49 < .58
100	.47 < .54 < .62
110*	.45 < .48 < .51
200*	.69 < .74 < .79
400**	.95 < 1.0 < 1.05

*$^2\Pi_{3/2}$

**Both spin states

Table 4b. V=1

P(mTorr)	$\phi_{corrected}$
14	.03 < .04 < .05
32	.06 < .08 < .10
48	.09 < .11 < .13
56	.12 < .14 < .16
75	.22 < .26 < .28
75*	.20 < .22 < .24
99	.28 < .31 < .34
99*	.27 < .31 < .34
119	.33 < .37 < .42
119*	.26 < .30 < .34
157	.40 < .45 < .50
157*	.44 < .48 < .53
400**	.95 < 1.0 < 1.05

* $^2\Pi_{3/2}$

**Both Spin Stales

Table 4c. V=2

P(mTorr)	$\phi_{corrected}$
18	.028 < .037 < .046
19*	.059 < .067 < .076
21	.075 < .104 < .113
34*	.113 < .133 < .152
50	.149 < .158 < .177
61	.206 < .224 < .252
61*	.241 < .27 < .30
193	.57 < .60 < .64
400	.95 < 1.0 < 1.05

*$^2\Pi_{3/2}$

**Both spin states

Table 4d. V=3

P(mTorr)	$\phi_{corrected}$
11	.12 < .14 < .16
22*	.17 < .20 < .22
26	.22 < .25 < .28
32	.22 < .25 < .27
38*	.30 < .32 < .35
40	.38 < .42 < .46
56	.43 < .47 < .50
72	.49 < .54 < .58
93	.72 < .78 < .85
93	.64 < .70 < .77
101*	.61 < .66 < .71
112	.61 < .68 < .74
119	.66 < .70 < .78
146	.69 < .78 < .85
154*	.67 < .71 < .75
158	.72 < .78 < .83
158	.59 < .65 < .72
400**	.95 < 1.0 < 1.05

*$^2\Pi_{3/2}$

**Both Spin States

Table 4e. V=4

P(mTorr)	$\phi_{corrected}$
6	.055 < .069 < .080
11	.11 < .12 < .13
17	.11 < .13 < .15
31	.18 < .21 < .23
42	.21 < .24 < .26
49	.28 < .30 < .34
75	.34 < .39 < .43
86	.42 < .47 < .52
108	.54 < .59 < .65
138	.49 < .54 < .60
160	.60 < .67 < .74
400	.95 < 1.0 < 1.05

All $^2\Pi_{3/2}$

Table 4f. V=5

P(mTorr)	$\phi_{corrected}$
15	.09 < .14 < .20
22	.24 < .30 < .36
24	.24 < .29 < .33
33	.29 < .35 < .41
40	.25 < .33 < .42
45	.38 < .45 < .52
61	.46 < .56 < .66
74	.43 < .51 < .59
89	.46 < .54 < .68
116	.57 < .68 < .80
142	.63 < .71 < .82
400	.95 < 1.0 < 1.05

All $^2\Pi_{3/2}$

Table 4g. V=6

P(mTorr)	$\phi_{corrected}$
14	.21 < .24 < .27
24	.32 < .36 < .41
31	.43 < .49 < .55
44	.40 < .44 < .49
48	.49 < .55 < .61
61	.50 < .57 < .63
95	.58 < .64 < .72
123	.60 < .67 < .75
142	.46 < .54 < .63
156	.65 < .74 < .83
400	.95 < 1.0 < 1.05

All $^2\Pi_{3/2}$

Table 4h. V=7

P(mTorr)	$\phi_{corrected}$
14	.065 < .105 < .148
18	.24 < .28 < .31
30	.35 < .41 < .46
30	.32 < .36 < .39
41	.41 < .45 < .49
70	.55 < .60 < .68
113	.51 < .59 < .67
400	.95 < 1.0 < 1.05

All $^2\Pi_{1/2}$

Table 5. Observed NO(v) Distributions: Low pressure and at 400 mTorr of O_2

V	[NO(v)] at .4 Torr O_2 (% of total)	[NO(v)], Low Pressure (% of total)	k_1^v, cm^3 $molecule^{-1}sec^{-1}$ based on $\sum_{o}^{7} k_c^v$ = .9 E-16
0	63.3	57.8	5.20 E-17
1	8.87	4.21	3.79 E-18
2	8.24	5.71	5.14 E-18
3	4.50	6.89	6.20 E-18
4	5.51	5.83	5.25 E-18
5	3.61	6.46	5.81 E-18
6	2.98	6.63	5.97 E-18
7	2.92	6.48	5.83 E-18

Table 6. Comparison of Calculated and Observed NO(v) Bandhead Ratios

V	Bandhead Ratio Observed	Calculated for 300 °K	Type of Ratio
0	.78±.05	.80	large $^2\Pi_{3/2}$: large $^2\Pi_{1/2}$
1	.59±.05	.64	large $^2\Pi_{3/2}$: large $^2\Pi_{1/2}$
2	.68±.05	.67	large $^2\Pi_{3/2}$: large $^2\Pi_{1/2}$
3	.93±.05	.96	large $^2\Pi_{3/2}$: small $^2\Pi_{1/2}$
4	Not Done		
5	.89±.08	.94	large $^2\Pi_{3/2}$: small $^2\Pi_{1/2}$
6	Not Done		
7	Not Done		

Table 7. Relevant Chemistry

Reaction	K (cm^3/sec) or (cm^6/sec)	$\tau=(k[A])^{-1}$ (msec)	A	Ref.
Creation				
$N(^4S) + O_2 \rightarrow NO(v) + O$	.9E-16	800-35000	O_2	1
Destruction				
$N(^4S) + NO \rightarrow N_2 + O$	3.4E-11	1.5	N	16
Quenching				
$NO(v) + O_2 \rightarrow NO(v-1) + O_2$	2.5E-14(v=1) 4.E-13(v=7)	3-124 .2-8	O_2 O_2	11,12 15
Negligible				
$NO(v) + O \rightarrow NO(v-1) + O$	6.5E-11	>13	O	17
$NO(v) + N_2 \rightarrow NO(v-1) + N_2$	1.7E-16	300	N_2	19,20,45
$NO(v) + Ar \rightarrow NO(v-1) + Ar$	1.1E-17	>1100	Ar	45
$NO(v) + NO(v') \rightarrow NO(v'') + NO(v'')$	>1.E-14	>E7	NO	45,46
$N(4S) + + O + M \rightarrow NO(v) + M$	1.1E-32	>E6	O	47
$N(^2D) + O_2 \rightarrow NO(v) + O$	5.2E-12	.01-1.	O_2	21
$N(^2P) + O_2 \rightarrow NO(v) + O$	2.6E-12	.02-2.	O_2	28
$N(^4S) + O_3 \rightarrow NO(v) + O_2$	5.E-16	>E7	O_3	48
$O + NO \rightarrow NO_2 + h\nu$	4.2E-18	>E8	O	49
$O + NO + M \rightarrow NO_2 + M$	7.E-32	>E5	O,M	49
$NO + NO + O_2 \rightarrow 2NO_2$	1.9E-38	>E11	NO,O_2	50
$NO + O_3 \rightarrow NO_2 + O_2$	1.5E-14	>4.E6	O_3	47
$NO + NO_3 \rightarrow 2NO_2$	7.4E-12	>E7	NO_3	51
$N + N + M \rightarrow N_2^* + M$	4.4E-33	1.E5	N, M	47
$O + O + M \rightarrow O_2 + M$	7.2E-33	>E6	O, M	52
$O + O_2 + M \rightarrow O_3 + M$	6.3E-34	1.2E3	O_2, M	53
$O + O_3 \rightarrow 2\ O_2$	8.9E-15	1.E5	O	47
$O_3 + NO_2 + M \rightarrow NO_3 + O_2 + M$	3.4E-17	>E7	O_3	47
$O + NO_2 \rightarrow O_2 + NO$	9.1E-12	100	O	54
$N_2(A) + N \rightarrow N_2(X) + N$	5.E-11	1.	N	28
$N_2(A) + O_2 \rightarrow N_2 + O_2$	7.7E-12	.01-1	O_2	36
$N_2(A) + O \rightarrow$ Products	1.5E-11	>67	O	55
$N + NO_2 \rightarrow N_2O + O$	1.4E-12	35	N	56
$NO_2 + NO_3 \rightarrow NO + NO_2 + O_2$	1.1E-15	>E7	NO_2,NO_3	50

Table 9 O_2 Quenching Rate Coefficients, k_2^v, and the calculated NO(v) Ratios Based on k_2^v at 400 mTorr O_2 Partial Pressure

v	K_2^v cm^3/molecule-sec from Ref. [9] (used in Table 7)	Chosen to fit 400 mTorr expt. data	Calculated NO(v) Ratios * from k_2^v taken from Ref [9]	best fit	Observed 400 mTorr O_2
0	---	---	19.1	17.3	17.5
1	2.5E-14	1.5E-14	2.67	2.1	2.5
2	5.5E-14	5.3E-14	2.58	2.3	2.3
3	1.1E-13	1.1E-13	1.8	1.4	1.2
4	2.5E-13	8.E-14	.83	1.63	1.5
5	1.8E-13	1.3E-13	1.	1.	1.
6	3.5E-13	1.2E-13	.41	.83	.83
7	2.0E-13*	7.6E-14	.33	.66	.81

*lower bound for k_2^7, Ref. [15]

*Entered relative to NO(v=5) population

Table 10 Comparison of the NO(v ≥ 2) Distributions Measured in Different Studies.

v	NO(v) / $\sum_{i=2}^{7}$ NO(v=i), in %						
	This Work		Rahbee and Givson			Whitson et al. [9]	
	Low Pressure	.400 Torr O_2	Calculated Nascent NO O Quenching	[10] With O Quenching	Measured 400 mTorr O_2	Calculated Nascent*	Measured 3 Torr O_2
2	15.0	29.7	30.4	25.	36.5	24.4	40.7
3	18.1	16.2	31.5	33.	32.0	15.8	27.1
4	15.3	19.8	18.2	19.	16.8	25.2	19.2
5	17.1	13.0	13.3	16.	9.8	22.6	9.35
6	17.3	10.8	3.87	4.1	3.4	7.3	2.68
7	17.1	10.4	2.76	3.3	1.4	4.7	.93

*Based on an analysis including O_2 quenching of NO(v), but omitting quenching of NO(v) by O.

Table 11: Comparison of Selected Kinetic Parameters for this Work and Previous IR Chemiluminescence Studies.

	$[O_2]$ mTorr	[N] molecules cm^3	[O] molecules cm^3	Reaction Time (msec)	Characteristic Times (msec) Removal by N Atoms**	Quenching by O†	Quenching by O_2*
This Work	50	2.E13	1.7E11	30.	1.5$^{\Delta}$	90.	6.2
This Work	400	2.E13	1.3E12	30.	1.5	12.	.78$^{\Delta}$
Rahbee et al. [10]	400	2.E13-7.E13	4.5E13	500.	.43-1.5	.34$^{\Delta}$	.78
Whitson et al. [9]	3000	1.6E13-5.E13	2.9E12	66.	.61-1.9	5.3	.10$^{\Delta}$

$^{\Delta}$ Principal process in the system

* Work was performed over a range of O_2 pressures from 200 - 600 mTorr. This pressure was chosen for purposes of comparison.

** a rate coefficient of 3.3E-11 cm^3/molecule sec was used
† a rate coefficient of 6.5E-11 cm^3/molecule sec was used
*a rate coefficient of 1.E-13 cm^3/molecule sec was used

Table 12: Einstein Transition Probabilities for $NO(X\ ^2\Pi, v)$ $\Delta v=1$ and $\Delta v=2$ IR Transitions $A_{v'v''}$ (sec^{-1})

v'	Fundamental	First Overtone
1	6.93	-----
2	13.6	1.07
3	20.1	3.03
4	25.3	5.77
5	32.5	9.2
6	38.6	13.3
7	44.4	18.1

from [57]

Table 13.

ATOMSPHERIC PARAMETERS OF IBC TYPE I AURORA

Altitude (km)	Temp. (neutral)	Temp (elect)	$[N_2]$	$[O_2]$	[NO]	[N]	[O]
85	1.80E+02	1.80E+02	9.20E+13	2.60E+13	9.70E+07	2.20E+03	1.00E+11
90	1.80E+02	1.80E+02	3.40E+13	1.10E+13	8.40E+07	1.00E+04	2.50E+11
95	1.90E+02	1.90E+02	1.20E+13	4.10E+12	7.00E+07	4.80E+04	2.50E+11
100	2.10E+02	2.10E+02	4.70E+12	1.50E+12	5.90E+07	2.20E+05	2.20E+11
105	2.35E+02	2.35E+02	2.10E+12	6.20E+11	5.00E+07	1.00E+06	1.80E+11
110	2.65E+02	2.65E+02	9.90E+11	2.60E+11	4.00E+07	1.20E+06	1.40E+11
115	3.10E+02	3.10E+02	4.90E+11	1.20E+11	3.30E+07	1.40E+06	9.80E+10
120	3.55E+02	3.55E+02	2.60E+11	6.00E+10	2.70E+07	1.60E+06	6.80E+10
125	3.90E+02	3.90E+02	1.50E+11	3.30E+10	2.20E+07	1.90E+06	4.89E+10
130	4.20E+02	4.30E+02	9.70E+10	2.00E+10	1.80E+07	2.30E+06	3.50E+10
135	4.50E+02	4.80E+02	6.30E+10	1.20E+10	1.45E+07	2.70E+06	2.70E+10
140	4.80E+02	5.45E+02	4.30E+10	7.70E+09	1.15E+07	3.20E+06	2.10E+10
150	5.30E+02	7.05E+02	2.10E+10	3.40E+09	7.60E+06	4.40E+06	1.30E+10
160	5.75E+02	9.15E+02	1.10E+10	1.70E+09	5.00E+06	6.00E+06	8.70E+09

Taken from Hurd *et al.* [43].

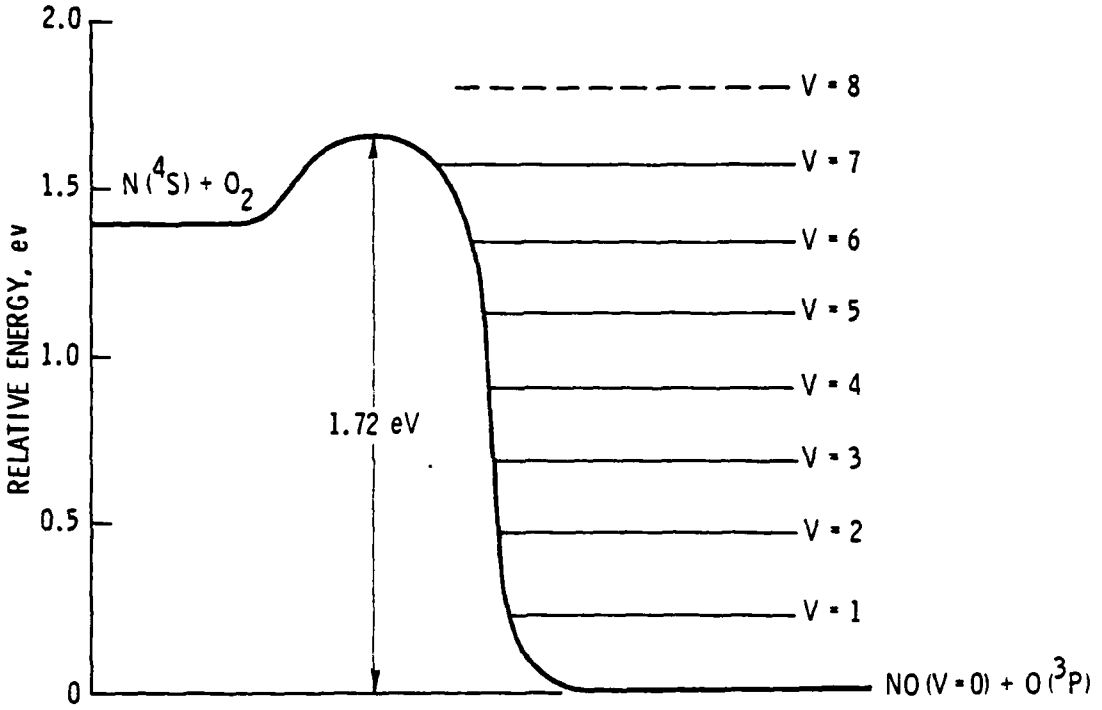

Figure 1. Energy Level Diagram for the $N(^4S) + O_2 (X^3\Sigma_g^-)$ Reaction

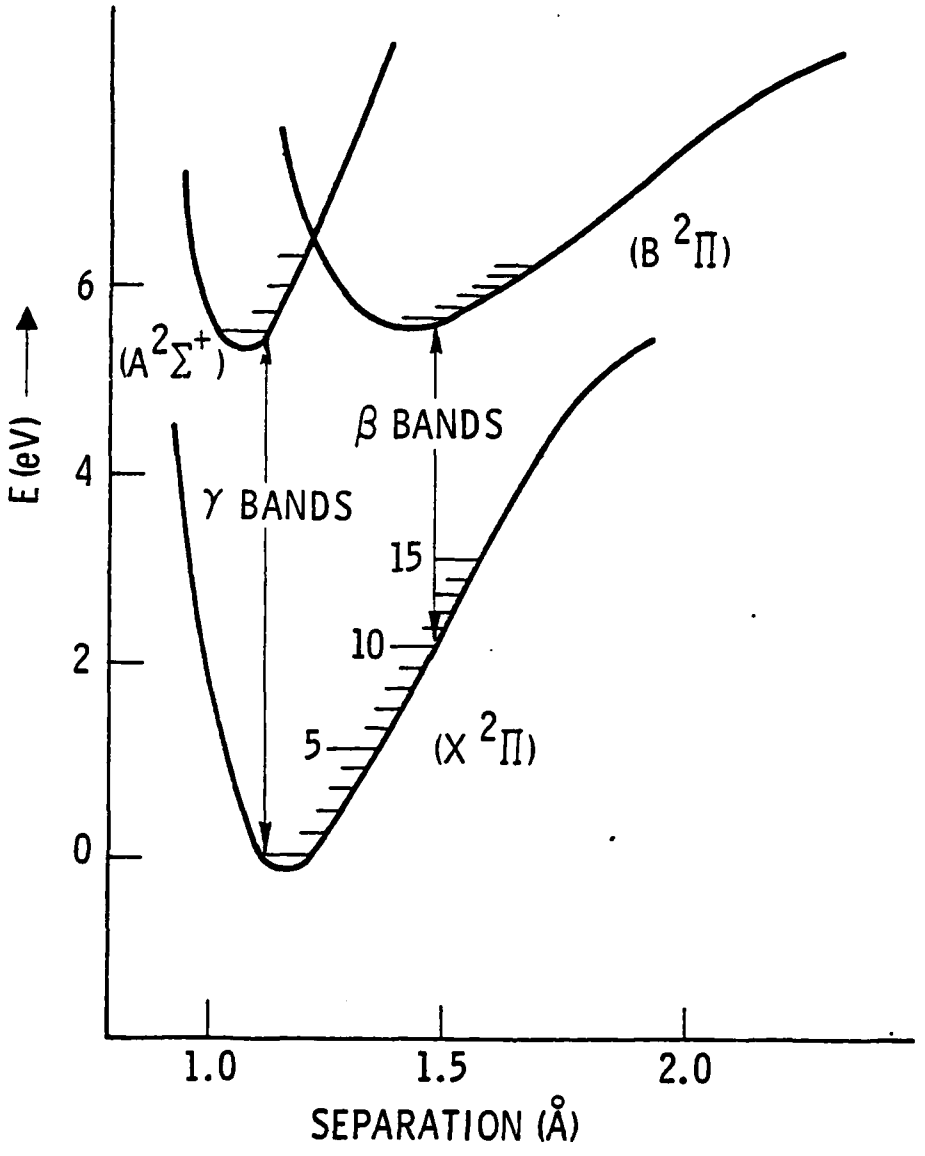

Figure 2. Electronic Energy Diagram of the NO Molecule (After Gilmore [58]).

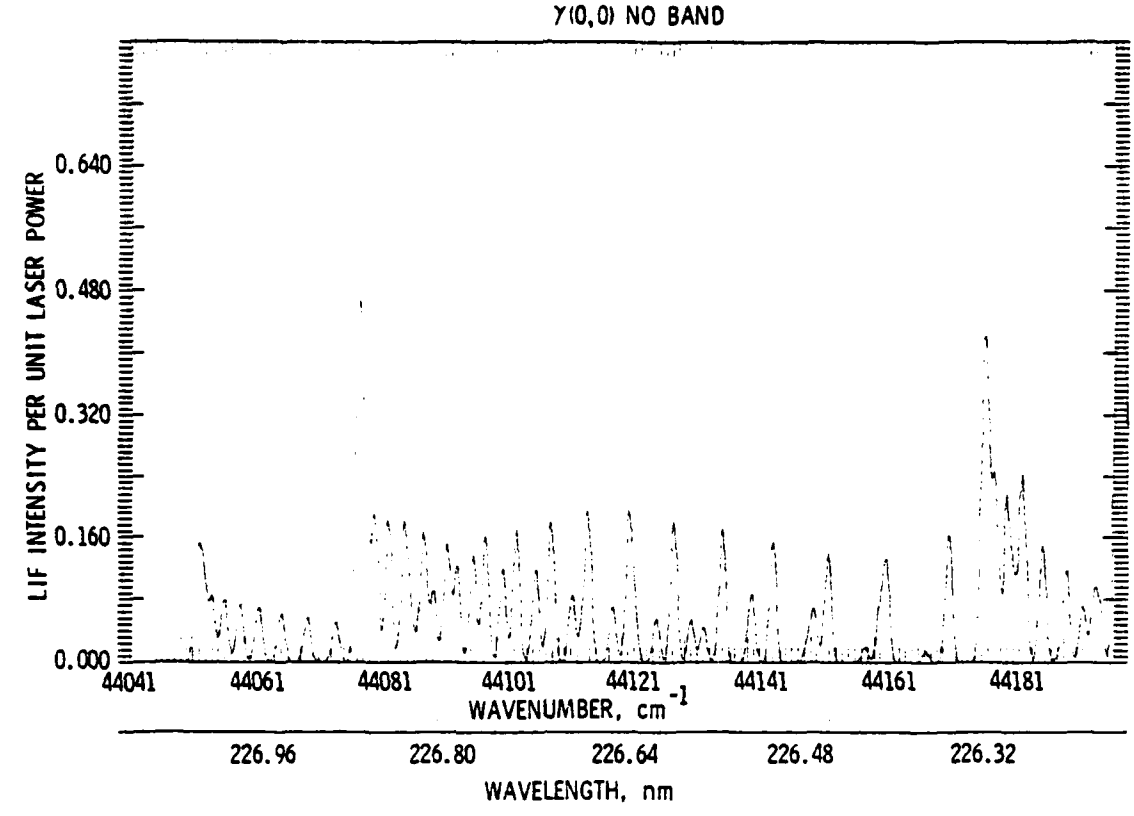

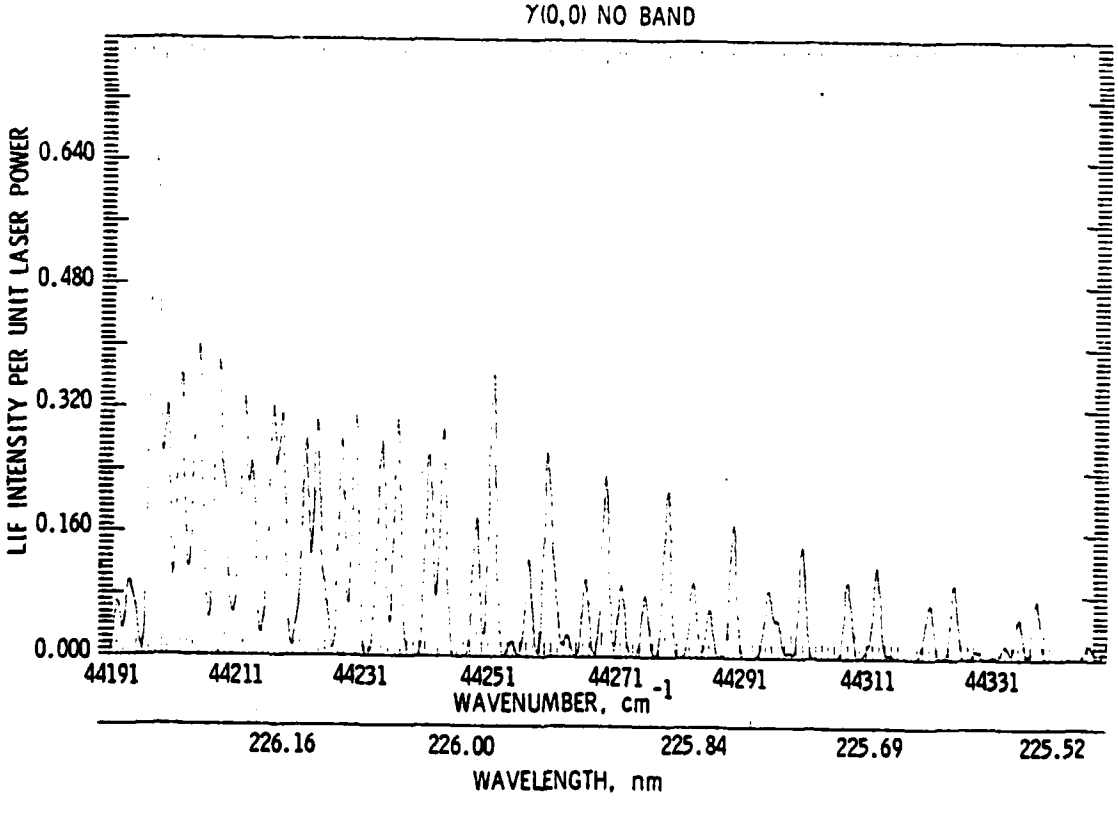

Figure 3. Calculated γ(0, 0) Excitation Spectrum

Table 8. Calculated Flowtube Composition for 50 mTorr and 400 mTorr O_2 Partial Pressure.

Species *	Concentration at 30 msec Reaction Time (Molecules/cm^3)	
	50 mTorr O_2	400 mTorr O_2
N_2	1.9E16	1.9E16
O_2	1.6E15	1.3E16
N	2.E13	1.9E13
Ar	8.9E16	7.7E16
O_3	6.4E6	1.49E10
NO*	0	4.3E8
O_2†	3.5E9	4.8E11
NO(v=0)	2.6E9	2.3E10
NO(v=1)	2.0E8	3.2E9
NO(v=2)	2.8E8	3.1E9
NO(v=3)	3.2E8	2.2E9
NO(v=4)	2.4E8	1.0E9
NO(v=5)	3.2E8	1.2E9
NO(v=6)	2.4E8	4.9E8
NO(v=7)	2.2E8	3.9E8
O	8.4E10	1.29E12

*Species having concentrations <1.E8, which are omitted from this list, include N_2O,NO_2, NO_3, NO(v=8), $N_2(A)$.

*From the reaction $O + NO_2 \rightarrow NO + O_2$

†O_2 which has quenched NO(v)

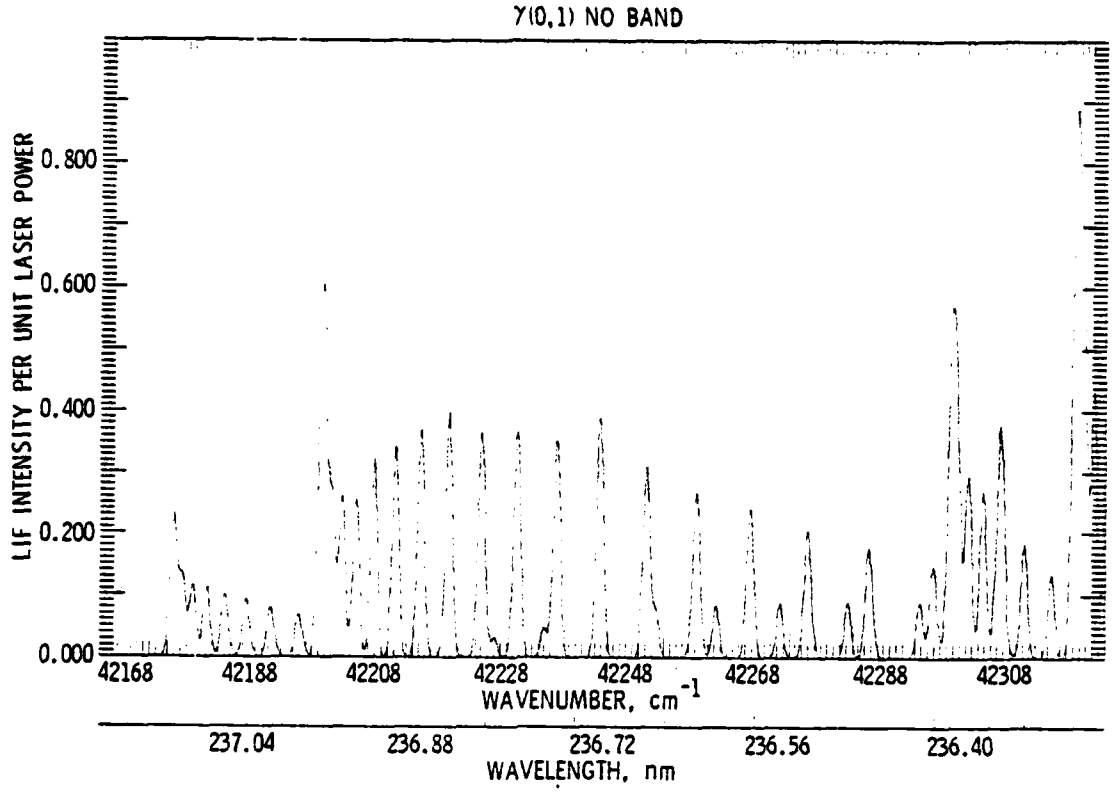

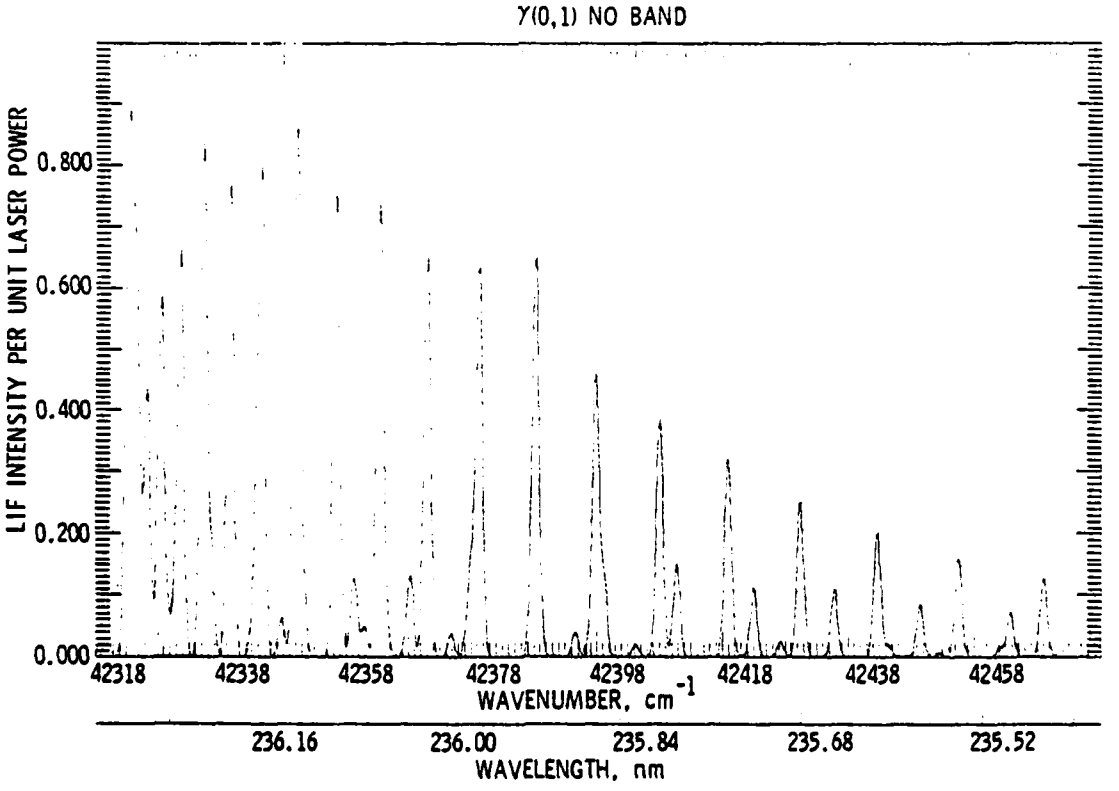

Figure 4. Calculated $\gamma(0,1)$ Excitation Spectrum

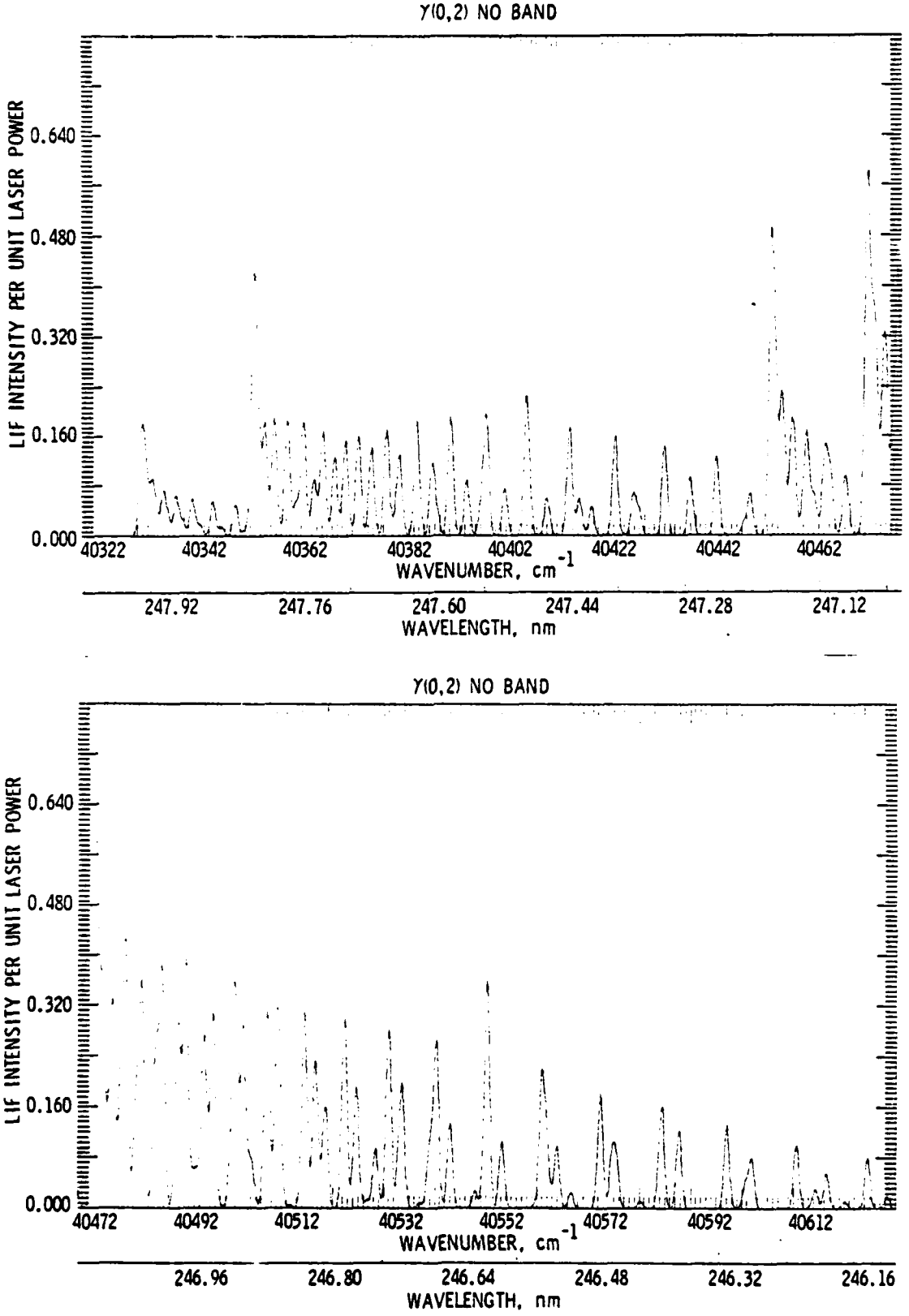

Figure 5. Calculated γ(0, 2) Excitation Spectrum

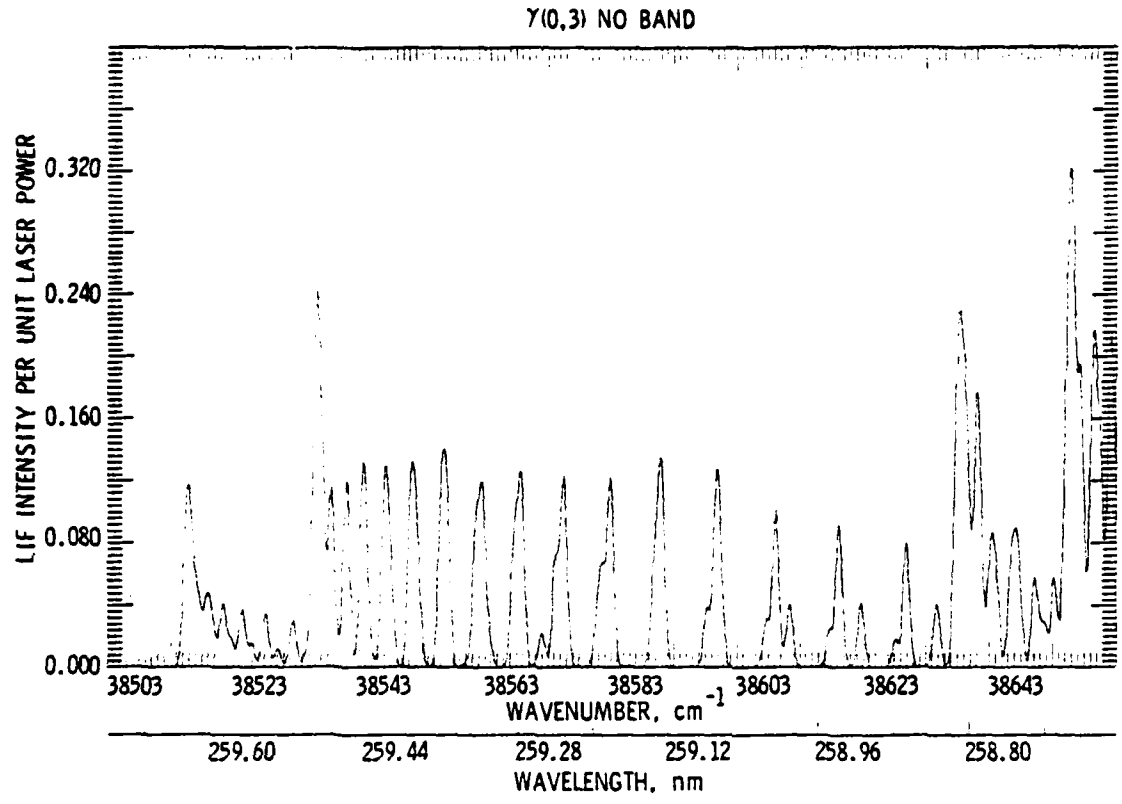

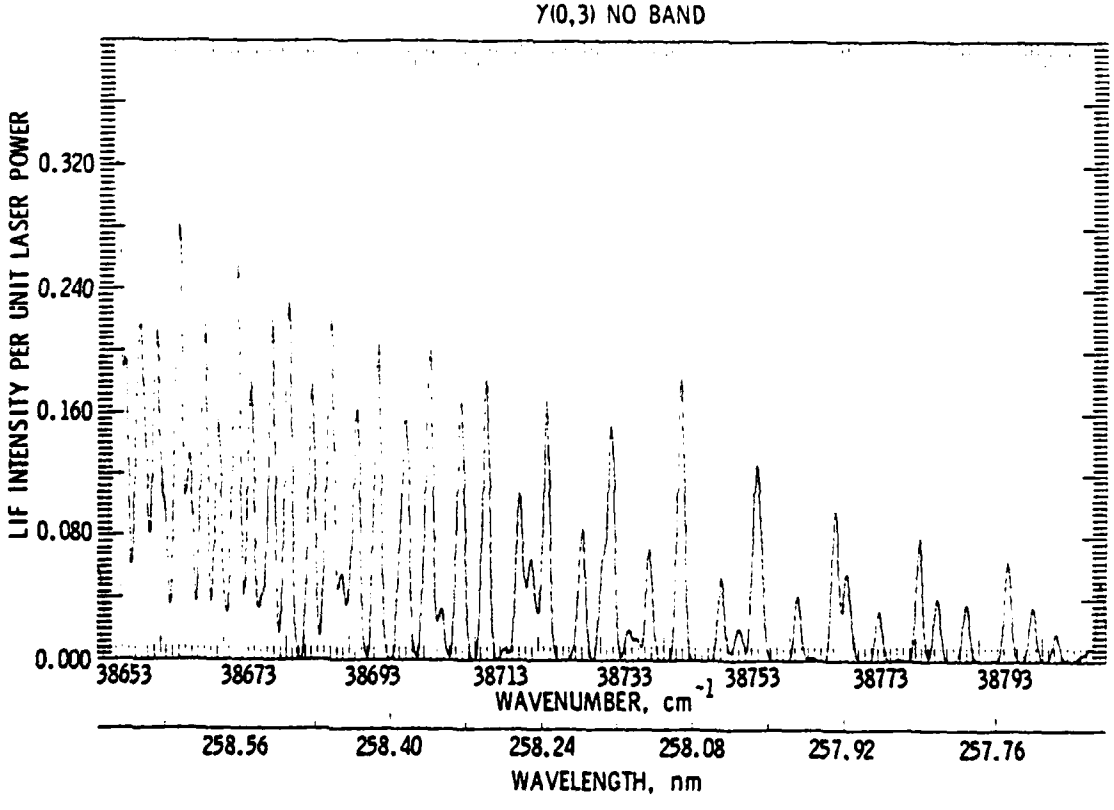

Figure 6. Calculated γ(0, 3) Excitation Spectrum

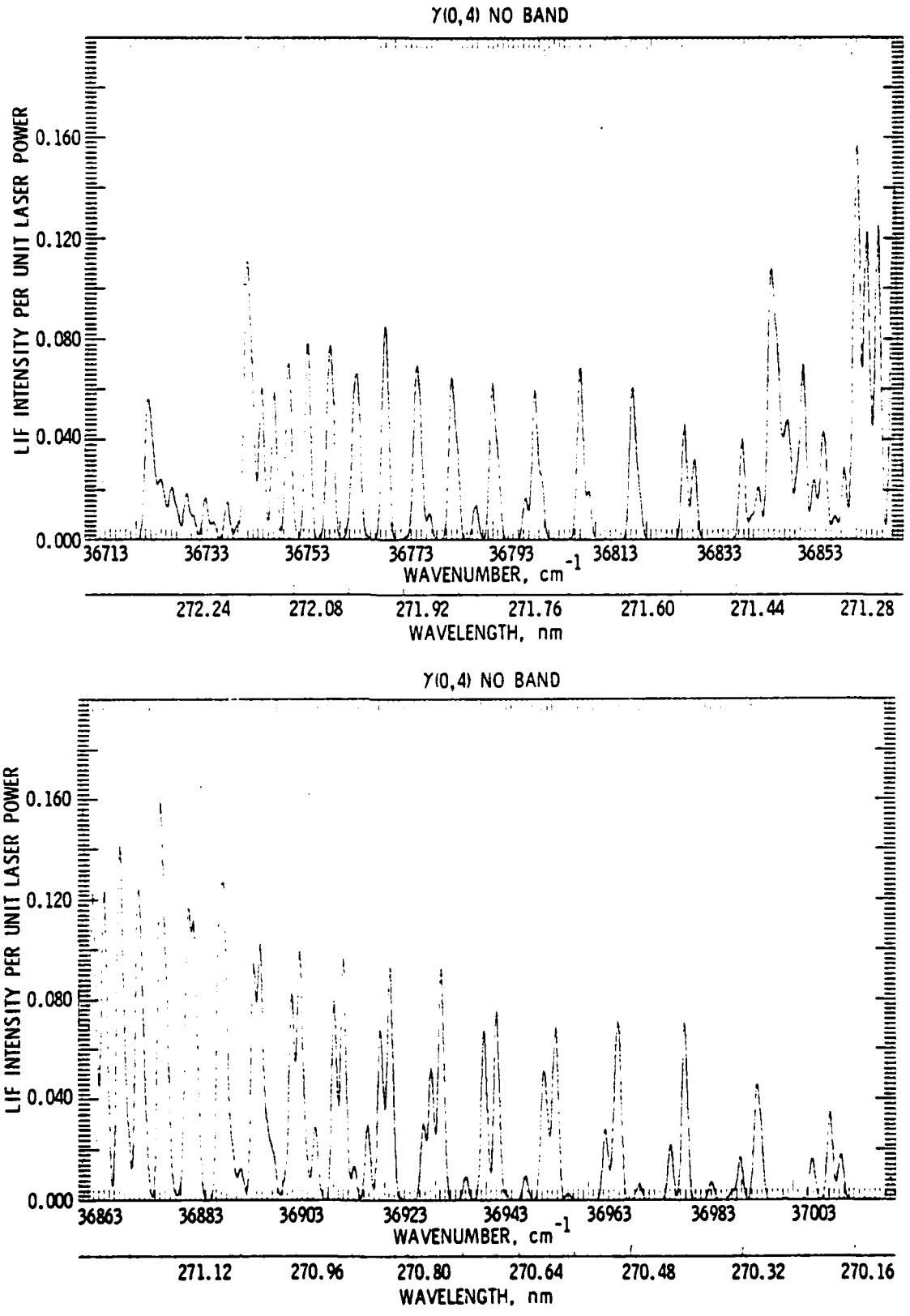

Figure 7. Calculated γ(0, 4) Excitation Spectrum

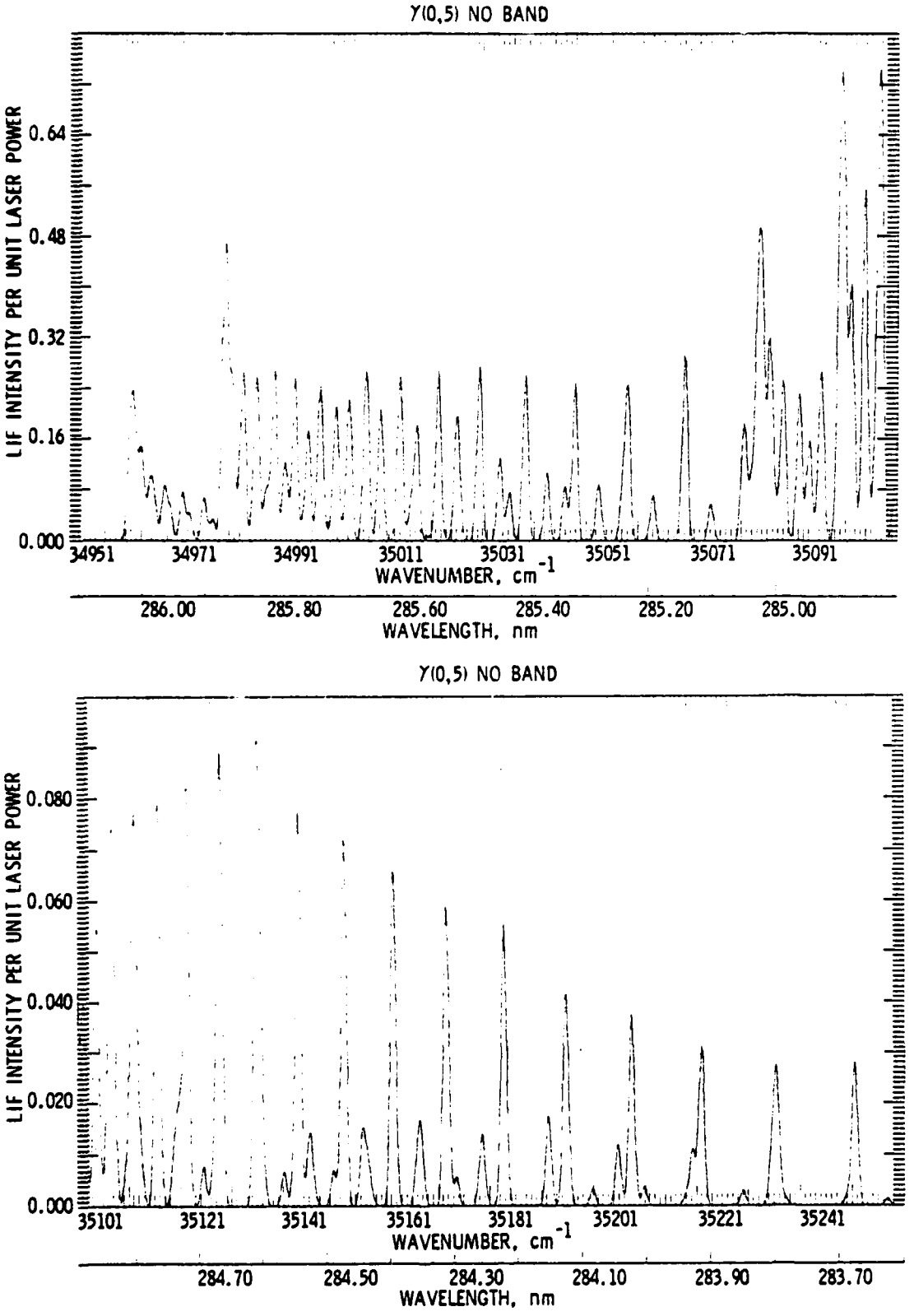

Figure 8. Calculated γ(0,5) Excitation Spectrum

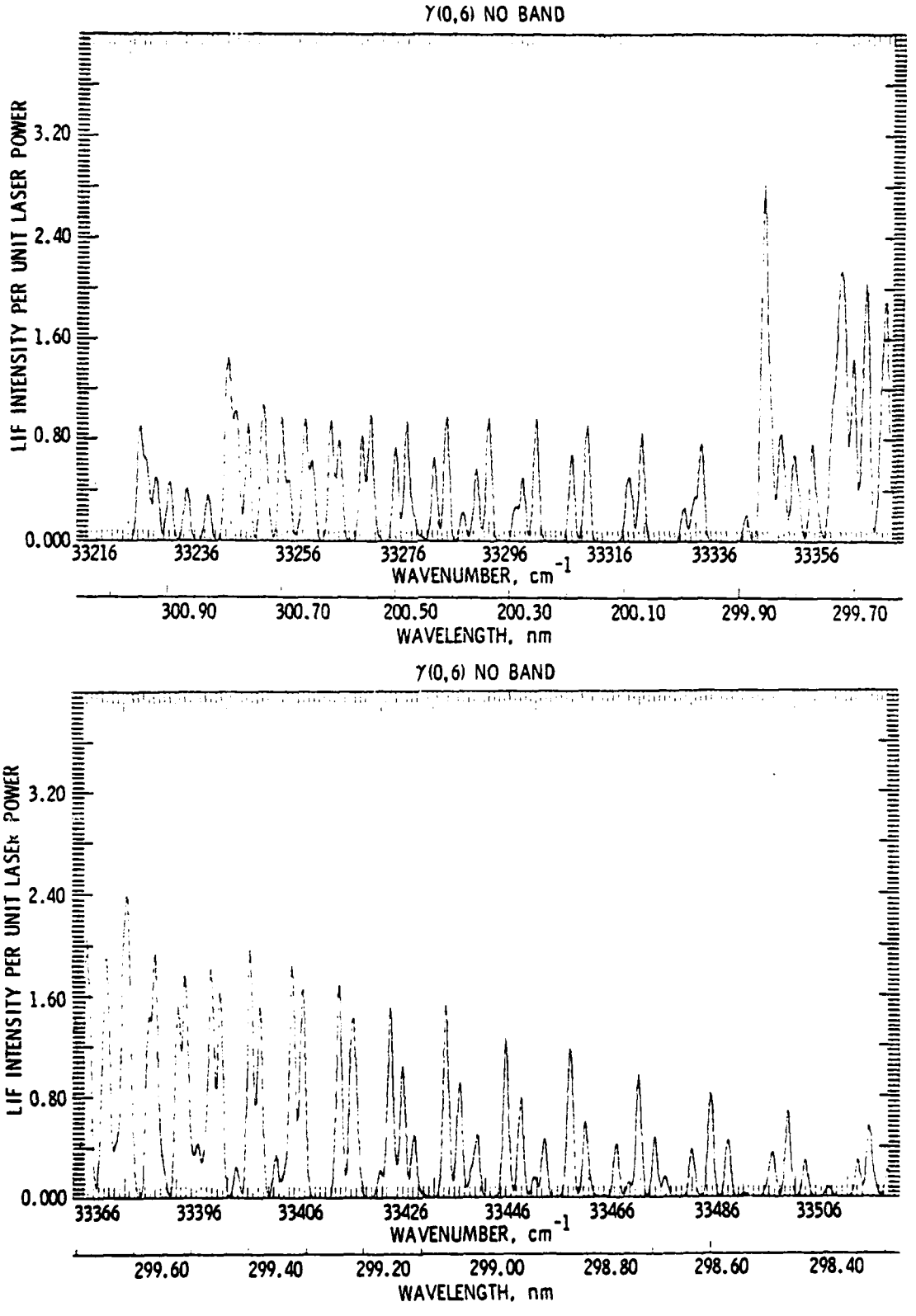

Figure 9. Calculated γ(0, 6) Excitation Spectrum

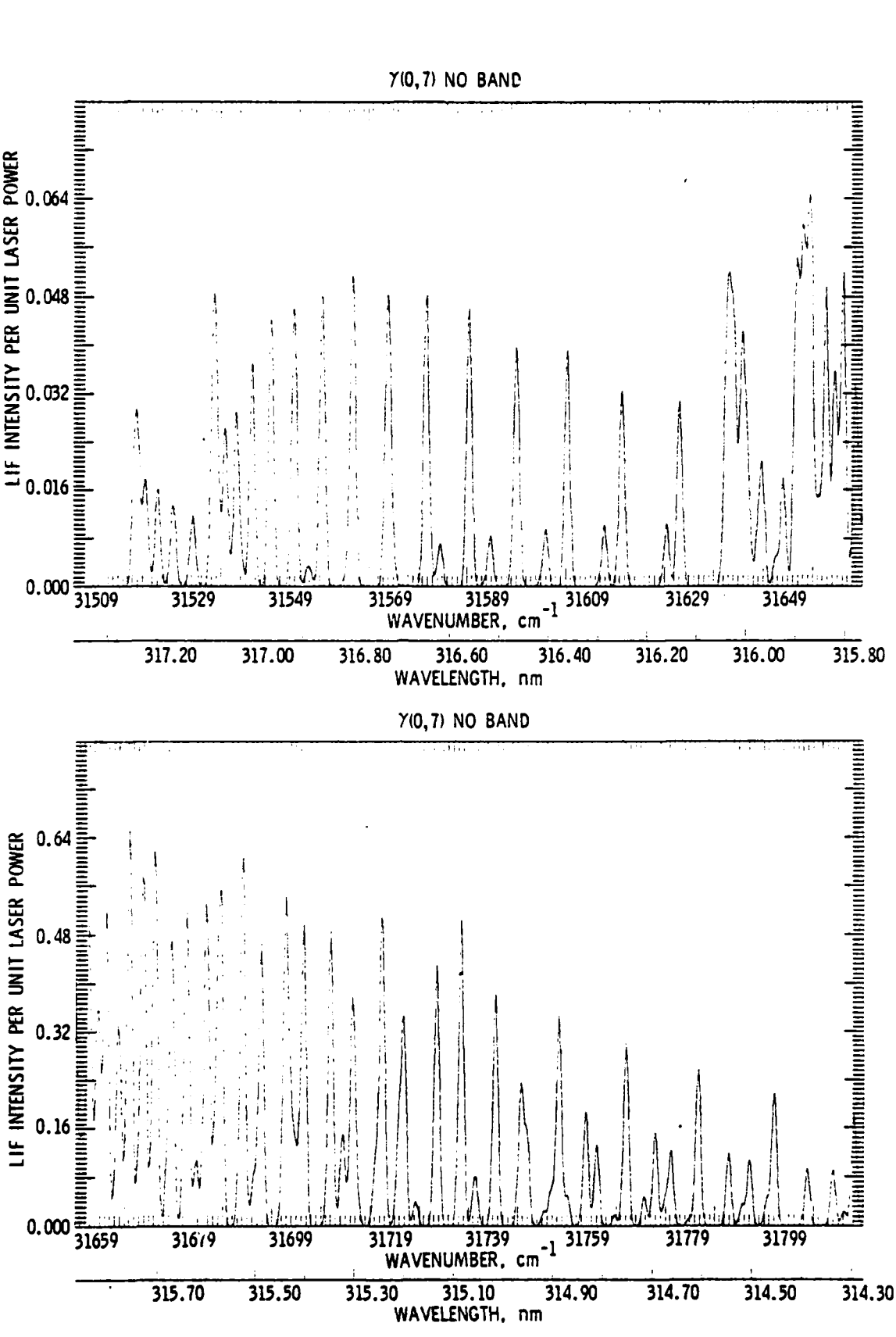

Figure 10. Calculated γ(0, 7) Excitation Spectrum

Figure 11. Schematic Diagram of the Apparatus

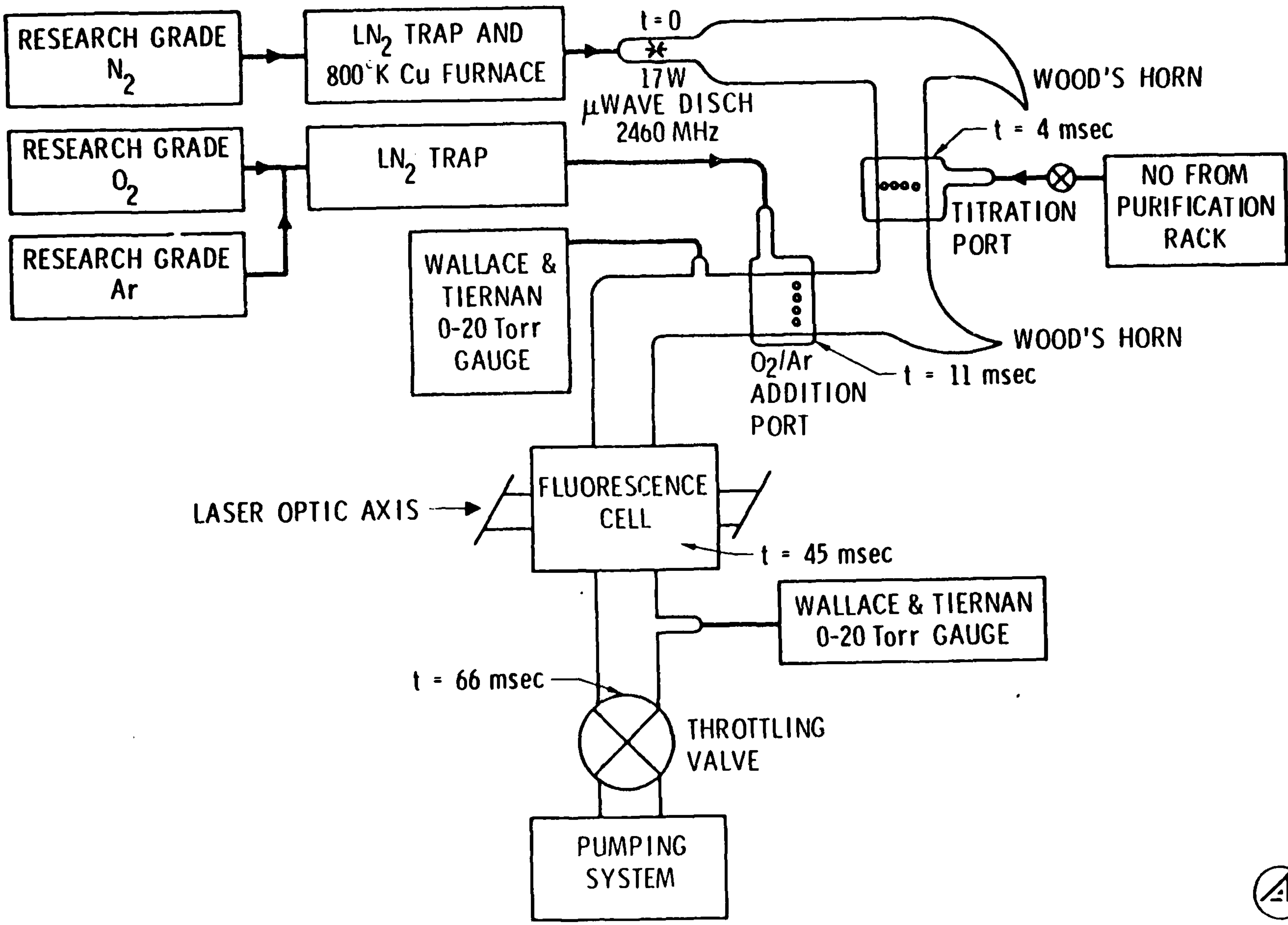

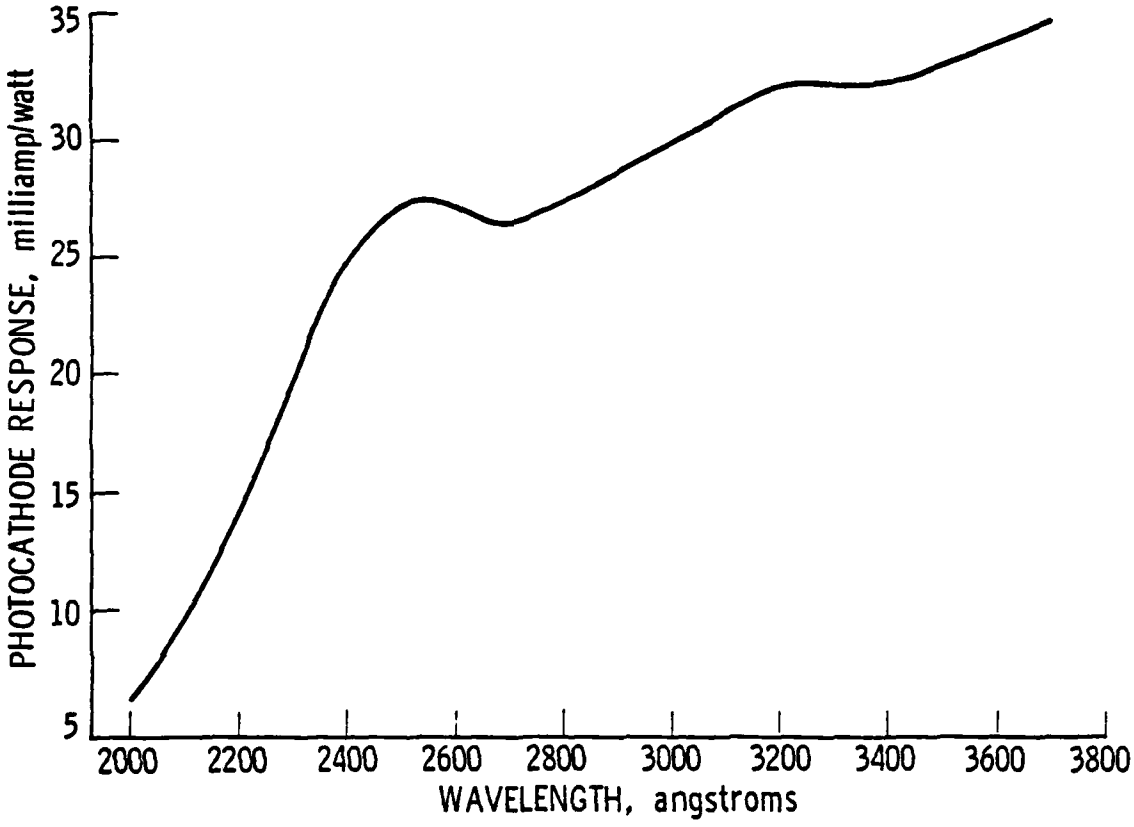

Figure 12. Spectral Response of the ITT Vacuum Photodiode

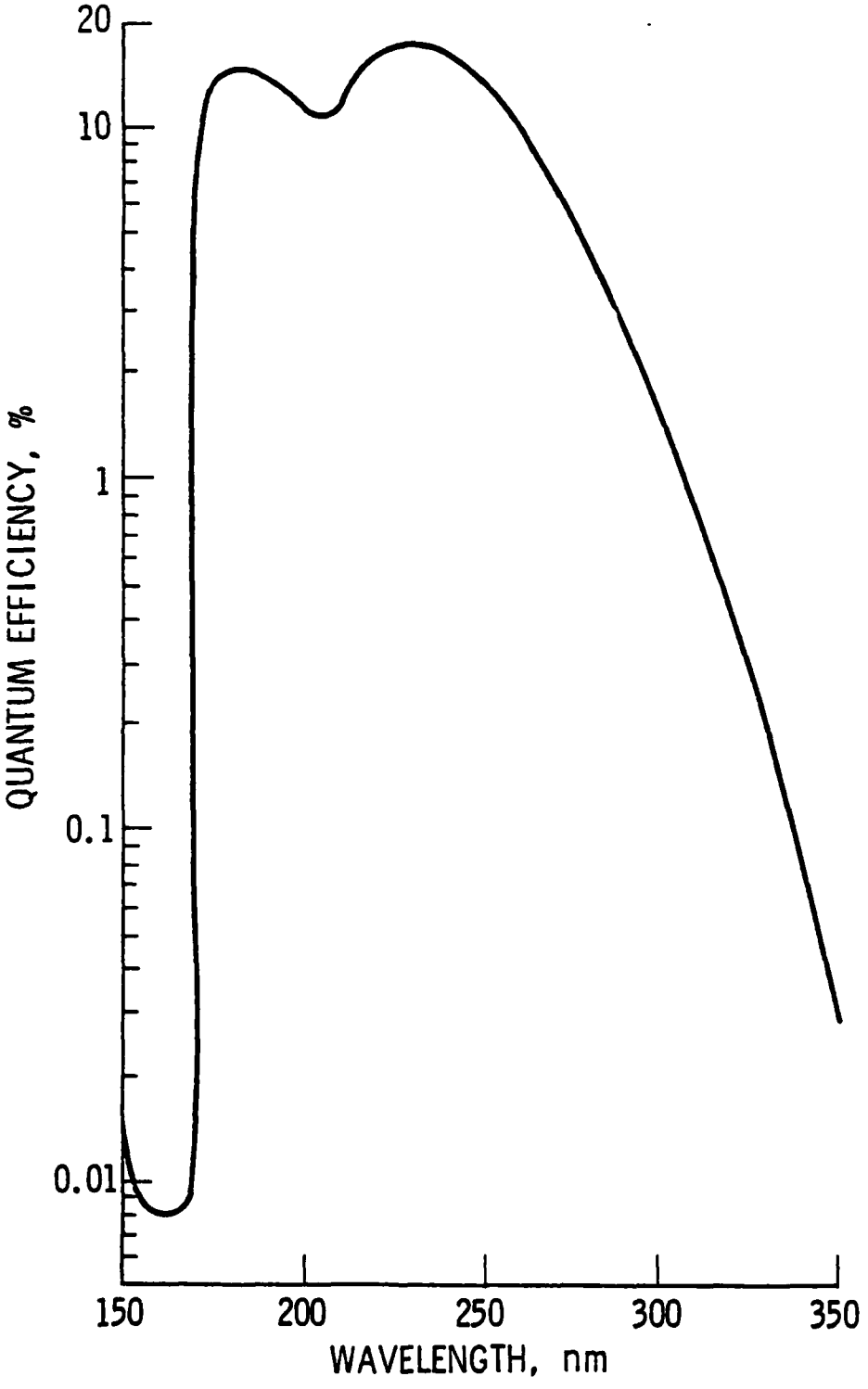

Figure 13. Spectral Response of the EMR 542 Q Solar Blind Photomultiplier

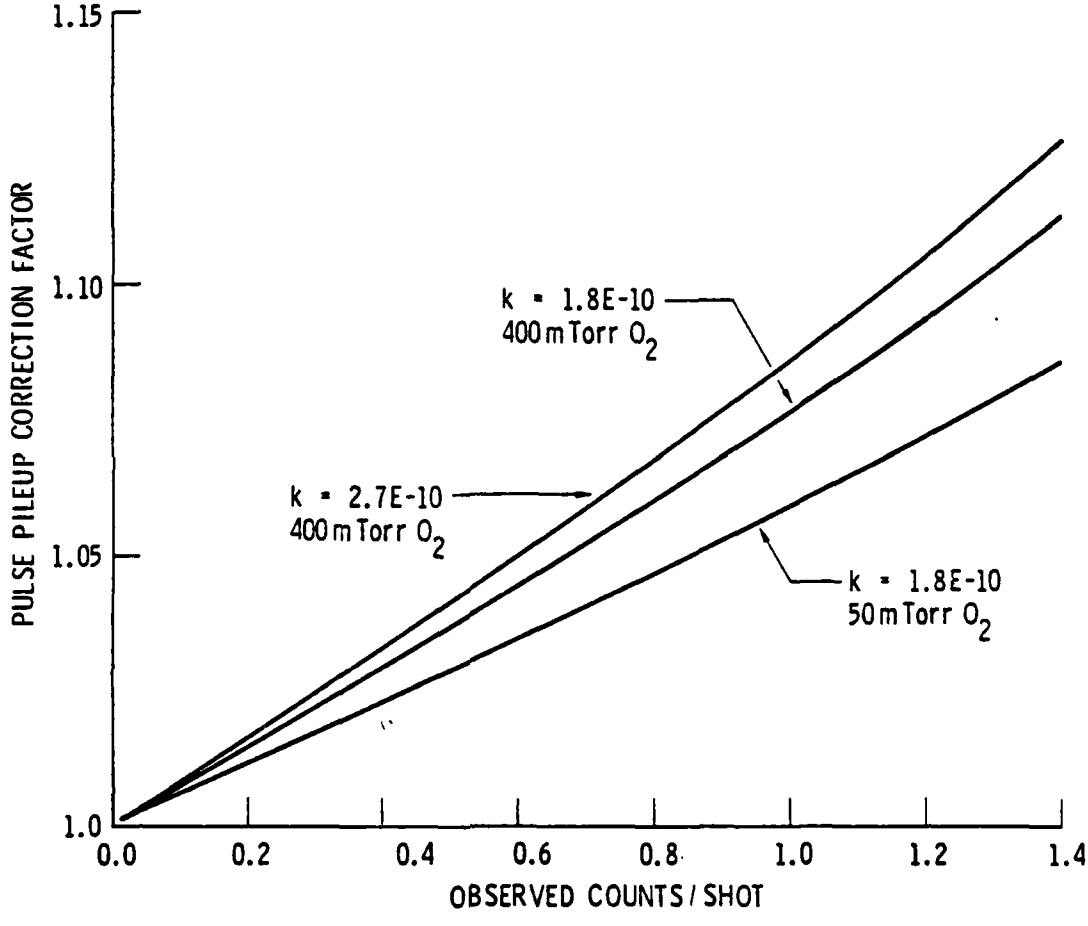

Figure 14. Pulse Pileup Correction Factors

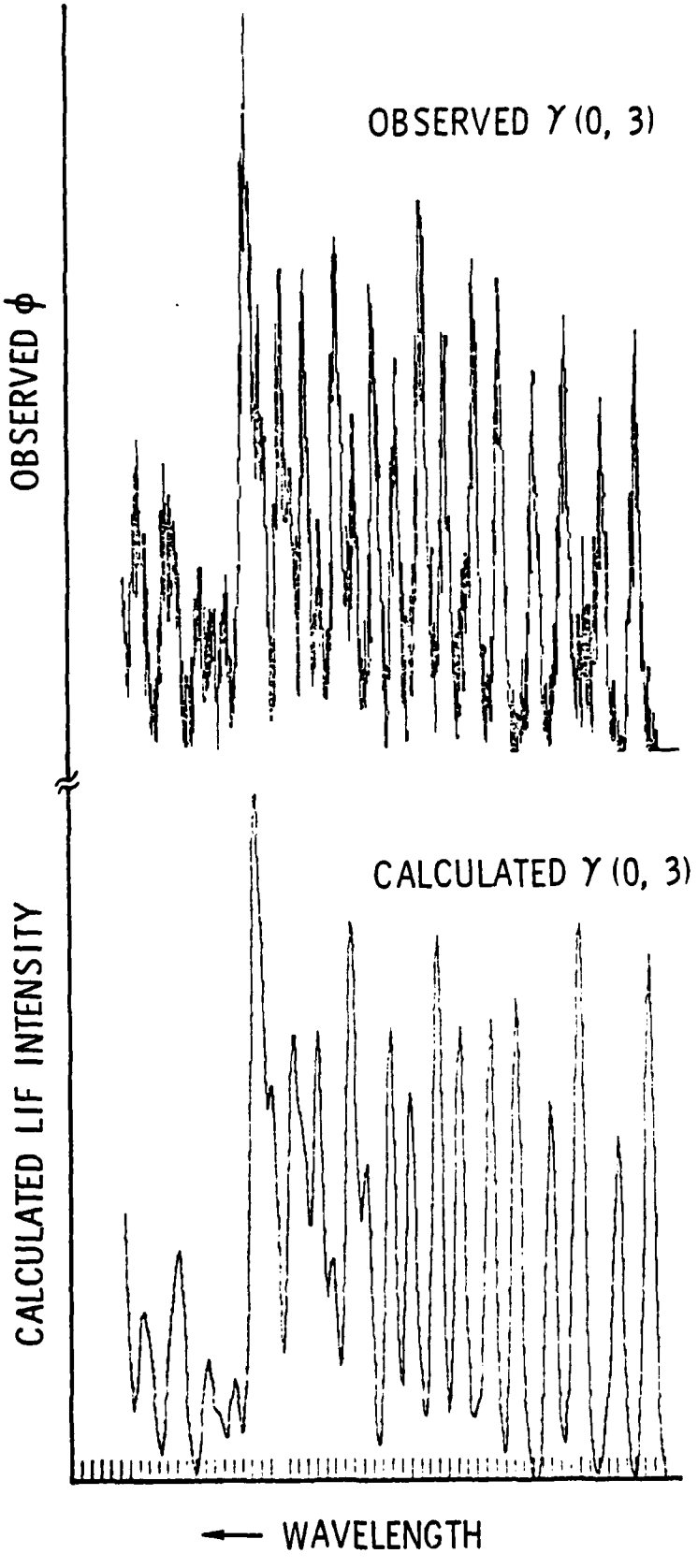

Figure 15. Comparison of the Observed $\gamma(0,3)\ ^2\pi_{1/2}$ Bandheads and the Spectrum Calculated Assuming 300° Equilibrium

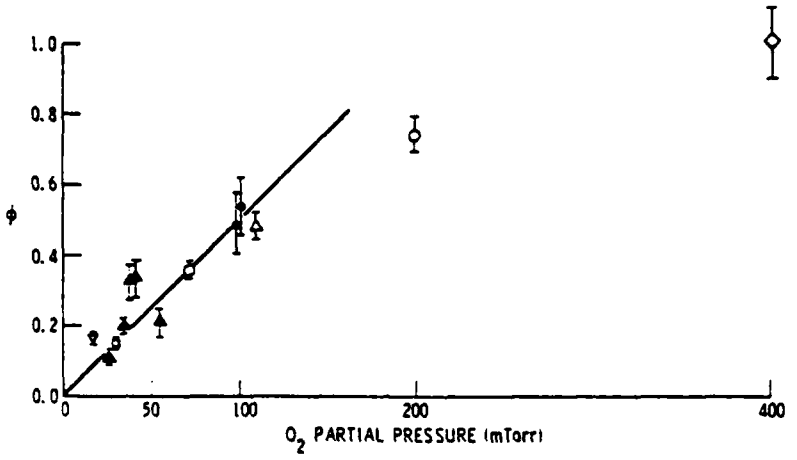

Figure 16. Experimental Results: v = 0. Open symbols = $^2\pi_{3/2}$. Closed symbols = $^2\pi_{1/2}$. Data from different days are denoted by different symbols.

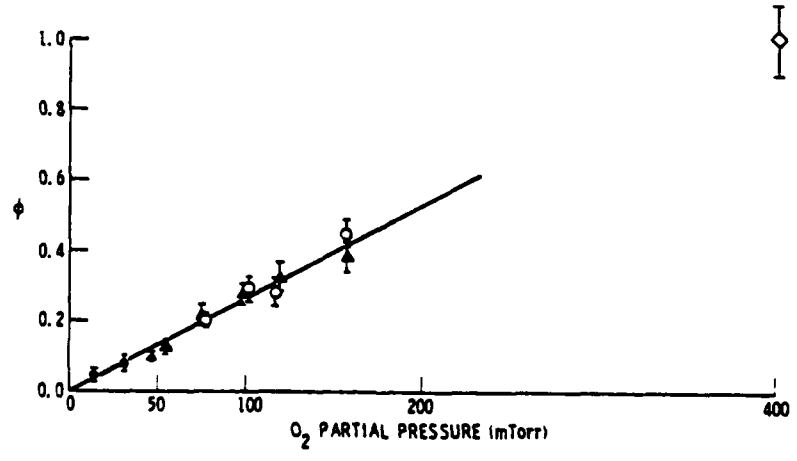

Figure 17. Experimental Results: v = 1. Open symbols = $^2\pi_{3/2}$. Closed symbols = $^2\pi_{1/2}$. Data from different days are denoted by different symbols.

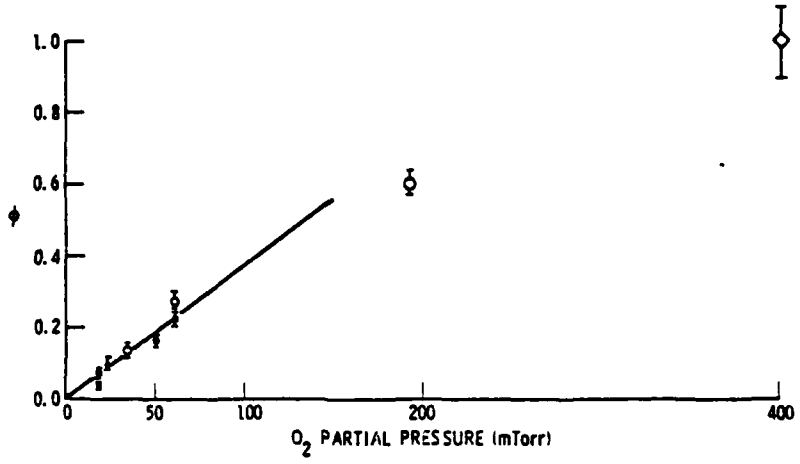

Figure 18. Experimental Results: v = 2. Open symbols = $^2\pi_{3/2}$. Closed symbols = $^2\pi_{1/2}$. Data from different days are denoted by different symbols.

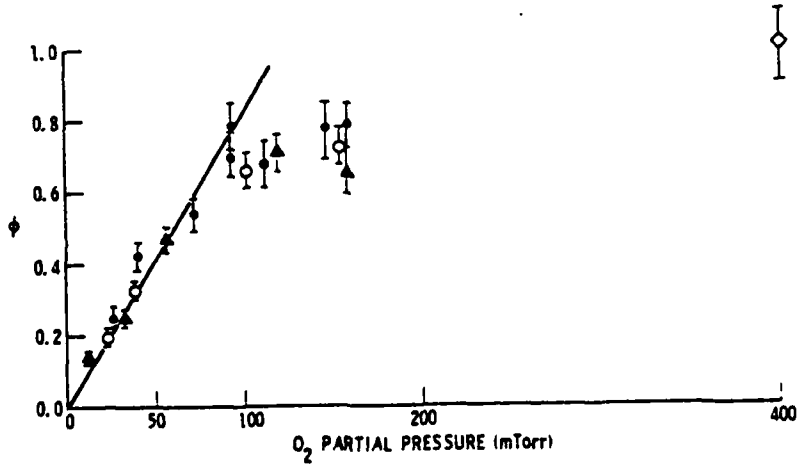

Figure 19. Experimental Results: v = 3. Open symbols = $^2\pi_{3/2}$. Closed symbols = $^2\pi_{1/2}$. Data from different days are denoted by different symbols.

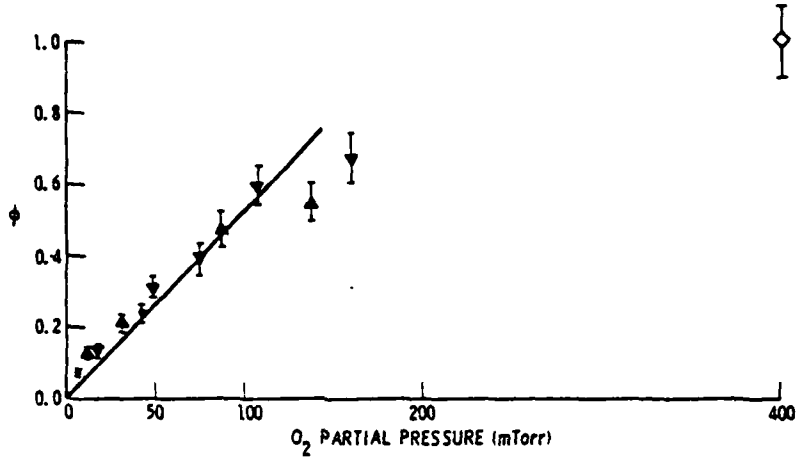

Figure 20. Experimental Results: v = 4. All $^2\pi_{1/2}$. Data from different days are denoted by different symbols.

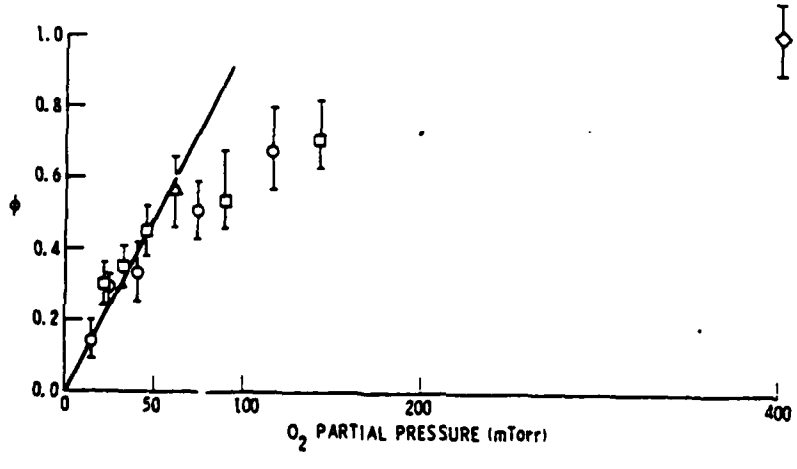

Figure 21. Experimental Results: v = 5. All $^2\pi_{3/2}$. Data from different days are denoted by different symbols.

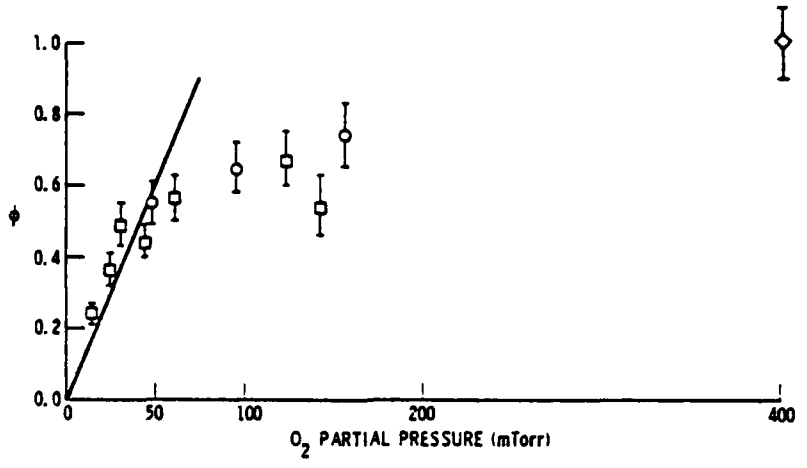

Figure 22. Experimental Results: v = 6. All $^2\pi_{3/2}$. Data from different days are denoted by different symbols.

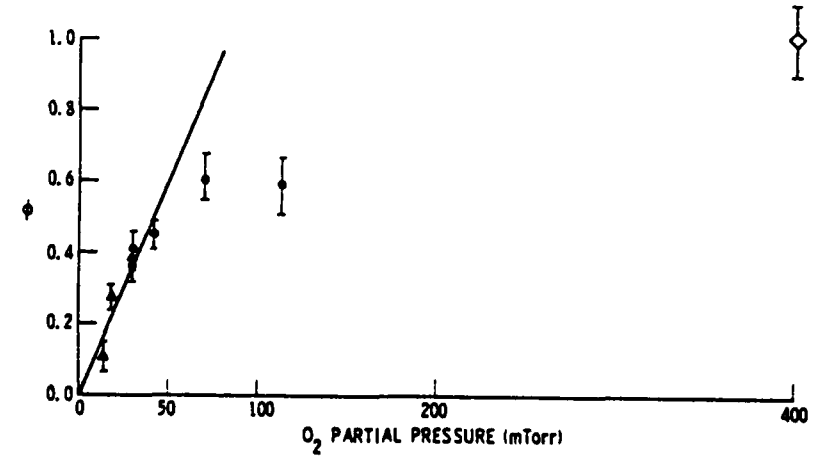

Figure 23. Experimental Results: v = 7. All $^2\pi_{1/2}$. Data from different days are denoted by different symbols.

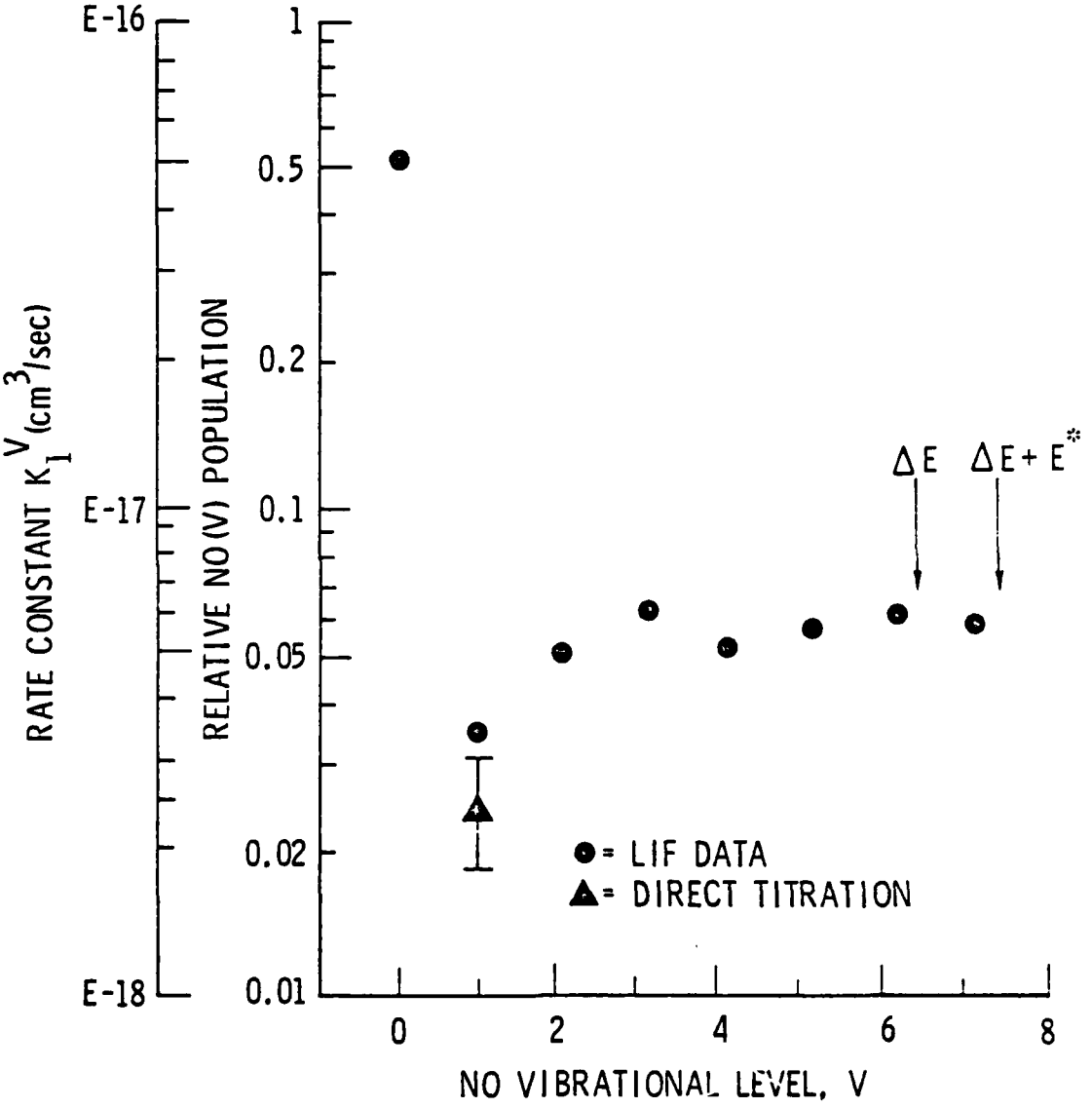

Figure 24. Observed NO Nascent Distribution. The Exothermicity, ΔE, and the Sum of ΔE and E^*, the Activation Energy, are Indicated to Show the Accessibility of V=7.

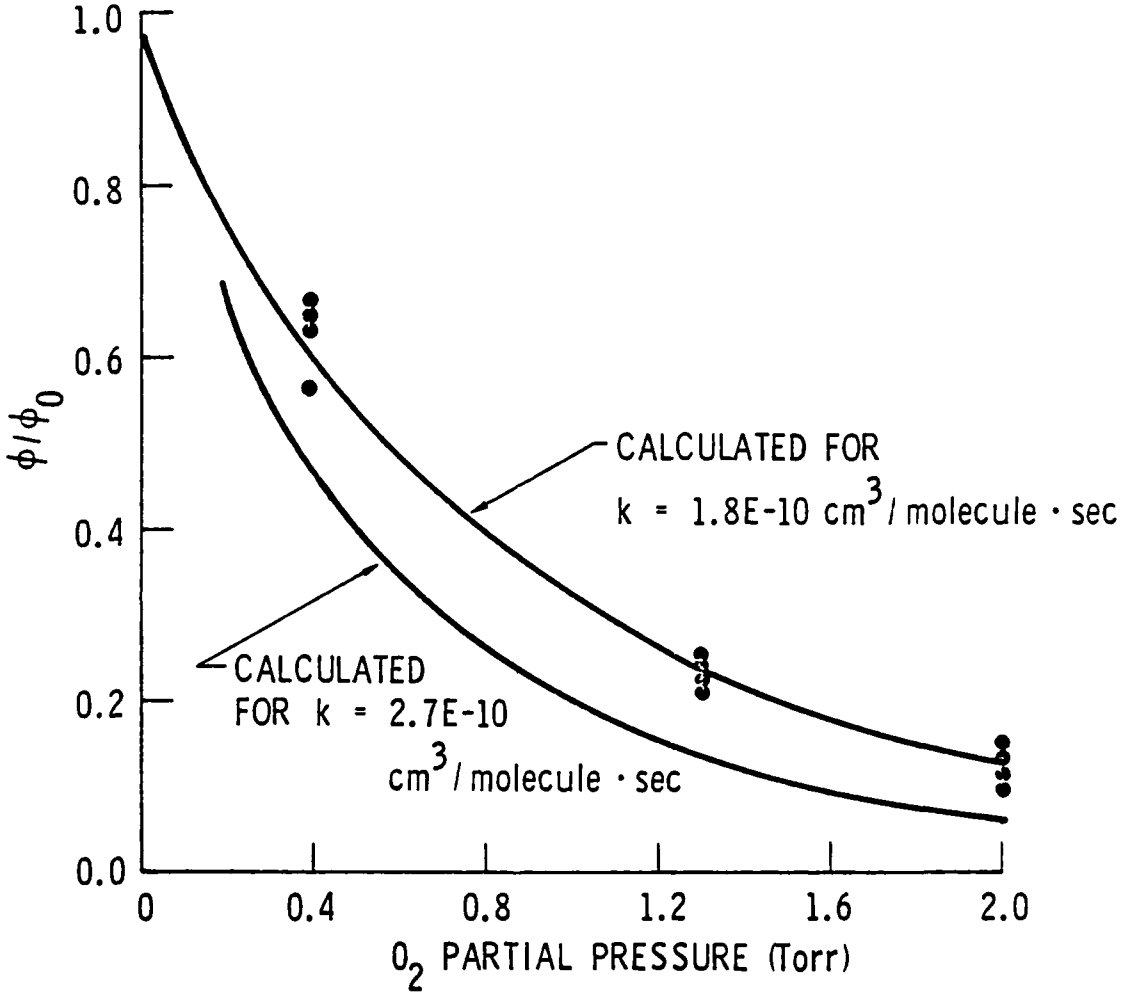

Figure 25. Observed Change in ϕ as a Function of O_2 Partial Pressure, for a Constant NO^2 Concentration.

AD-A111 889 UNIVERSITY OF SOUTHERN CALIFORNIA LOS ANGELES F/G 20/5
EXPERIMENTAL STUDIES OF THE STATE-TO-STATE CHEMICAL DYNAMICS OF--ETC(U)
NOV 81 R R HERM, B J SULLIVAN, M E WHITSON AFOSR-77-3348
UNCLASSIFIED AFOSR-TR-82-0102 NL

2 OF 2

END
DATE FILMED
4-82
DTIC

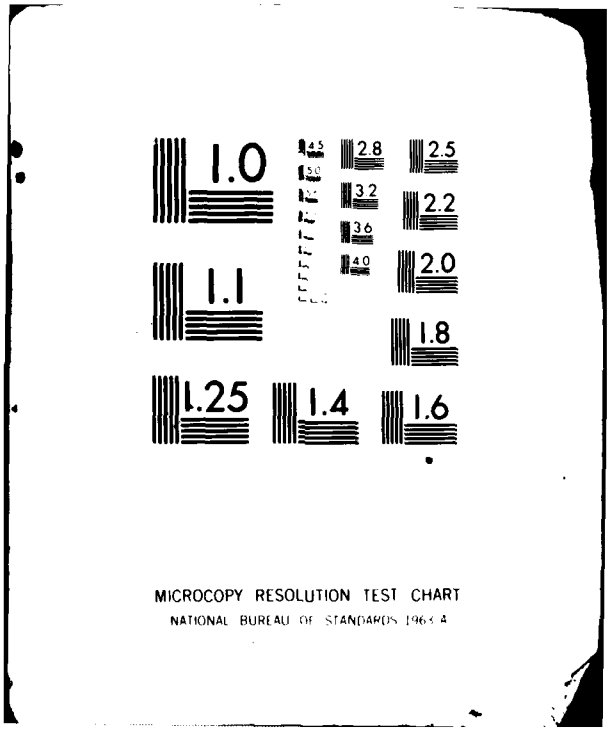
1.0
1.1
1.25
1.4
1.6
1.8
2.0
2.2
2.5
2.8
3.2
3.6
4.0
4.5
5.0
MICROCOPY RESOLUTION TEST CHART
NATIONAL BUREAU OF STANDARDS 1963 A

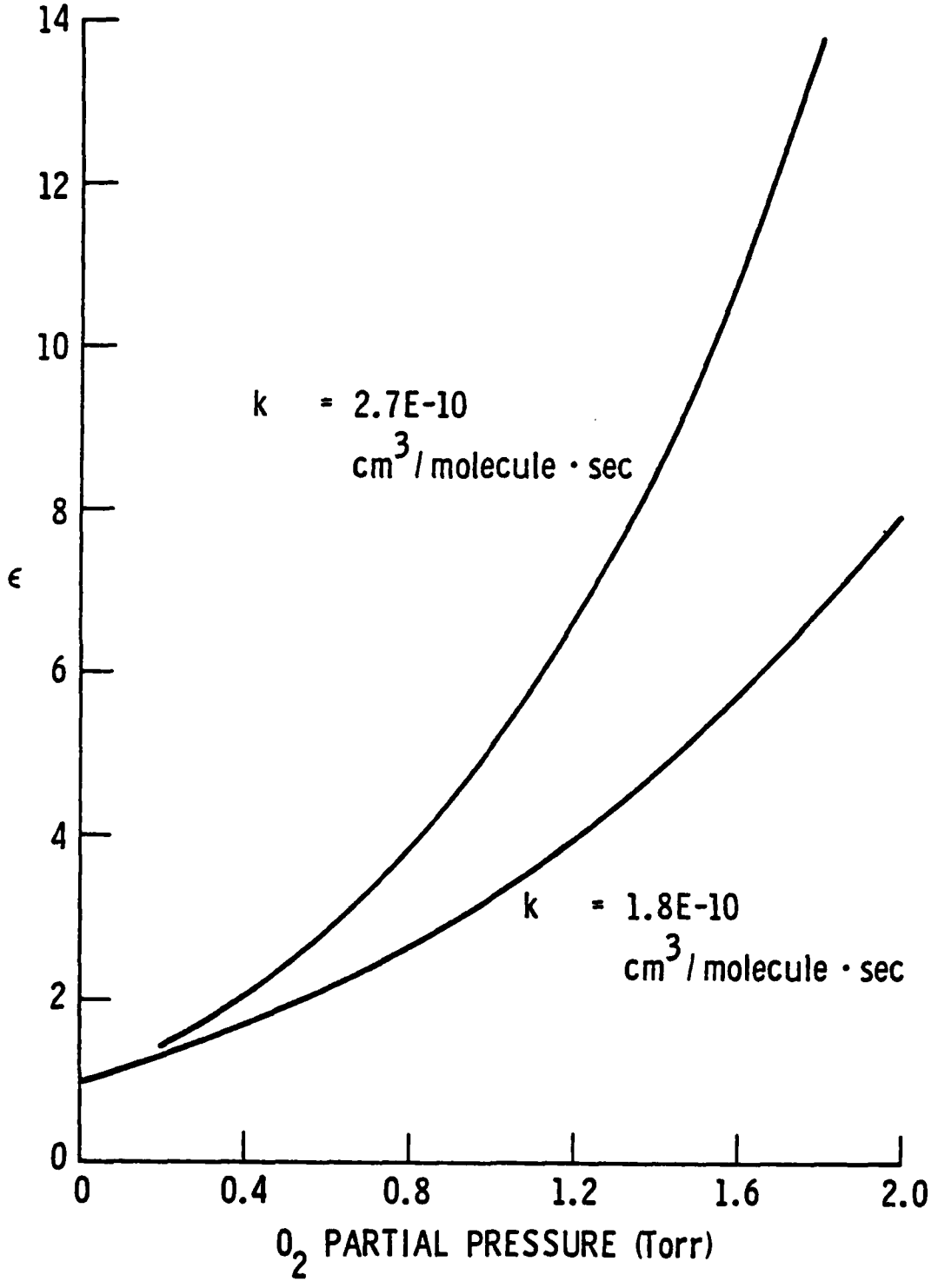

Figure 26. Fluorescence Efficiency Correction Factors, ϵ, for Two Values of k_{15}.

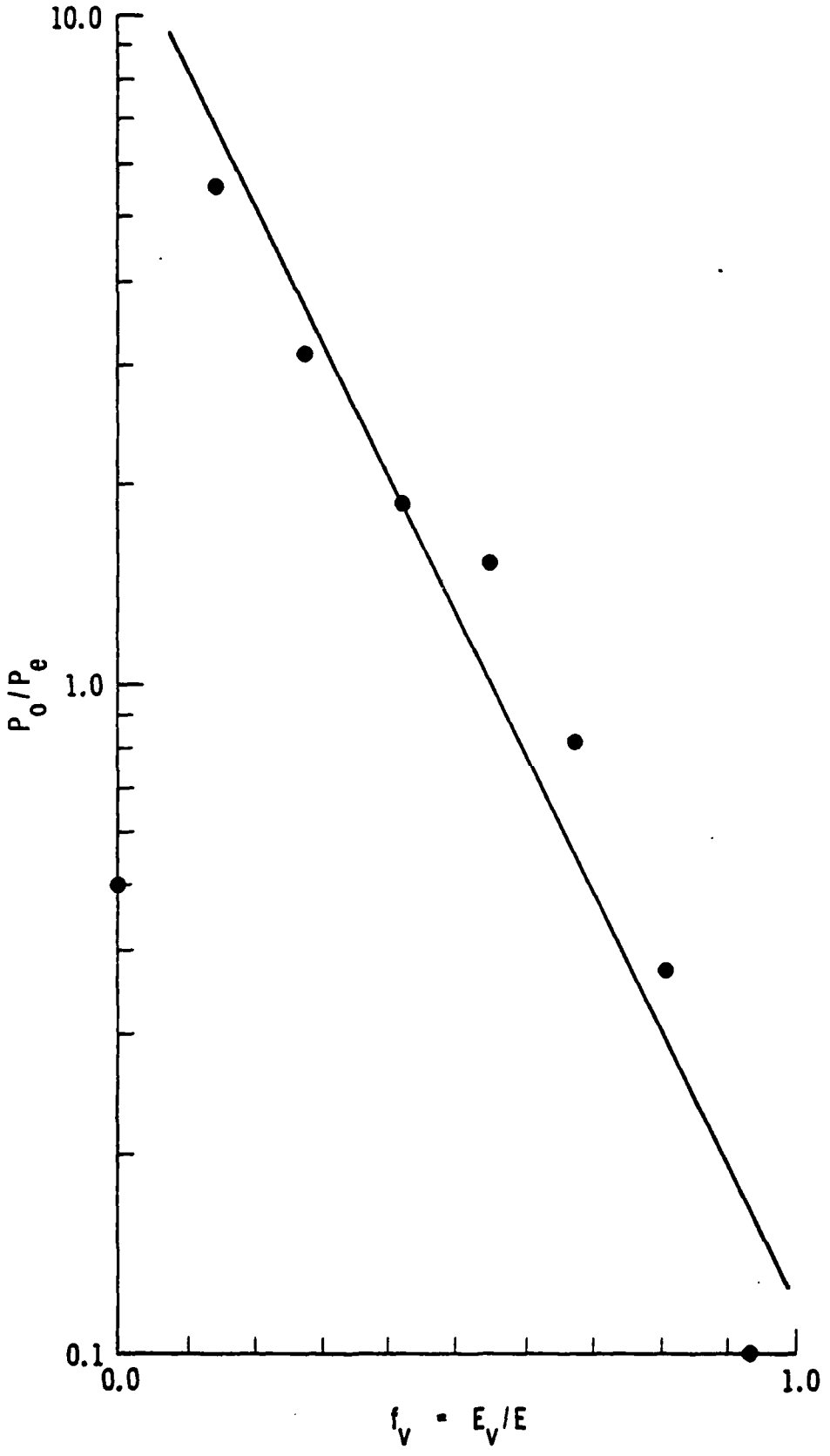

Figure 27. Surprisal Plot of the $N(^4S) + O_2$ Reaction.

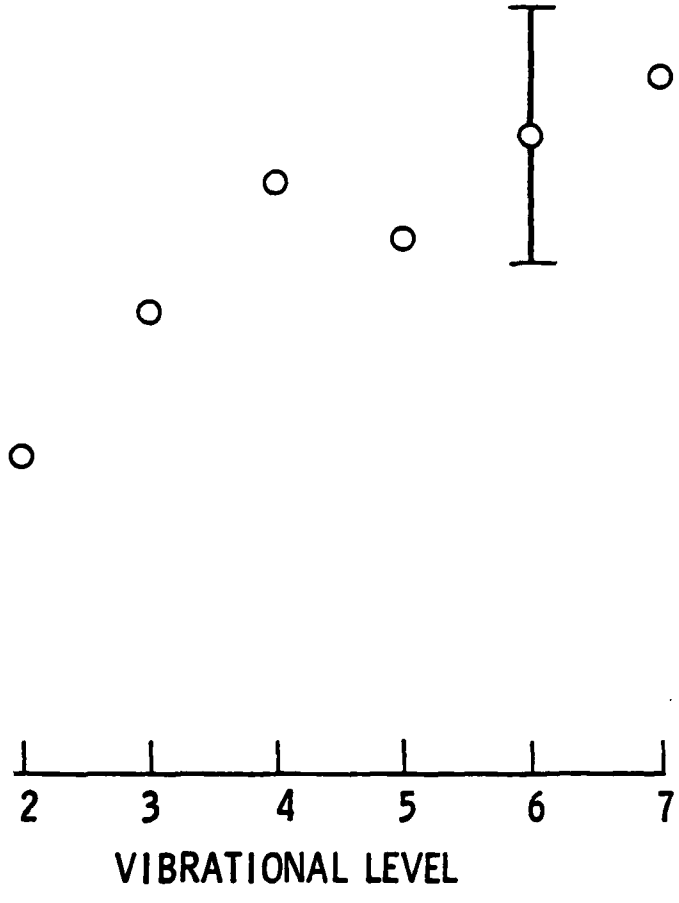

ion of the rate coefficient for NO(v) quenched by O_2,
nction of V, from Caledonia [15].

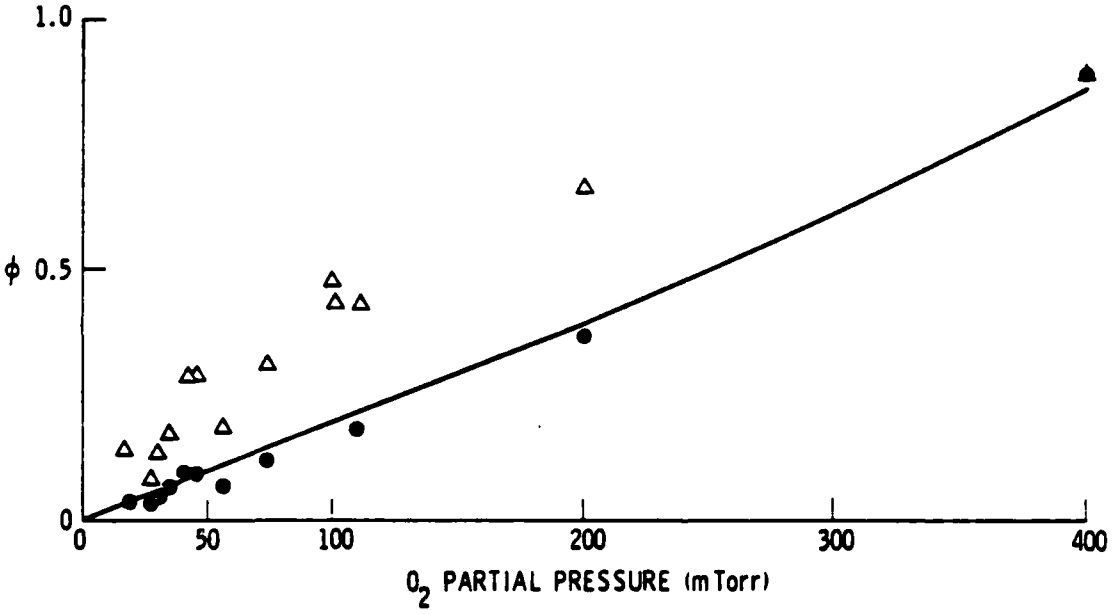

igure 29. Comparison of γ(0, 0) LIF Data Corrected for two values of k_{15}. Triangles are for k_{15}=1.8E-10 cm^3 $molecule^{-1}sec^{-1}$; dots are for k_{15}=5.E-10 cm^3 $molecules^{-1}$. The solid line is the calculated NO(v=0) variation with O_2 pressure obtained using the values of k_1^v reported in this work.

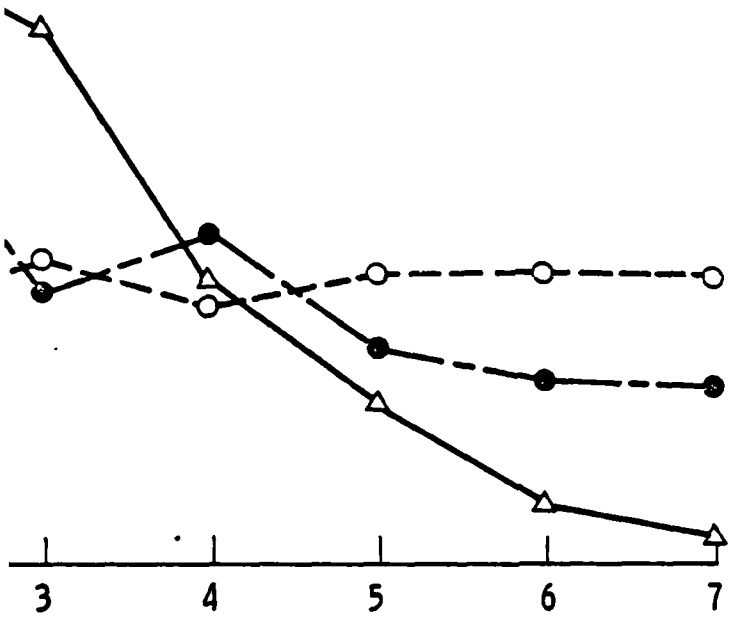

of 400 mTorr O_2 NO(v≥2) ratios. Δ=Rahbee and measured by IR chemiluminescence in an sphere. ● = this work. O = low pressure ratios,

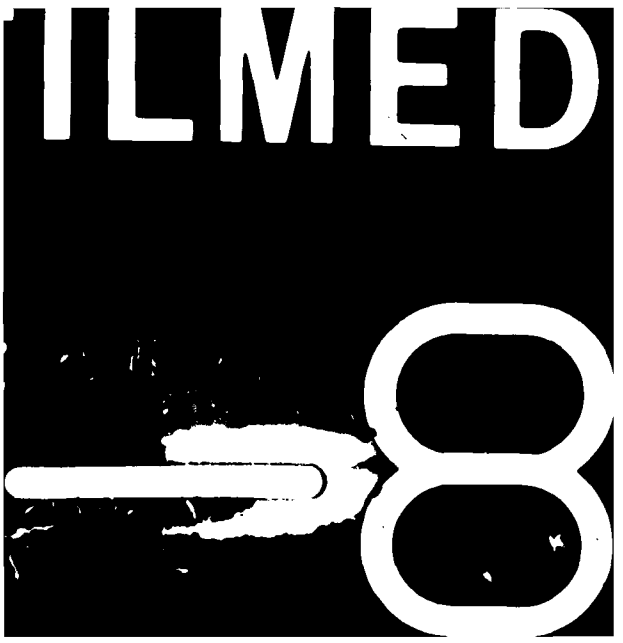
ILMED
8